NeuroImage 131 (2016) 55–72

Contents lists available at ScienceDirect

NeuroImage

journal homepage: www.elsevier.com/locate/ynimg

Full Length Articles

Advanced MRI techniques to improve our understanding of experience-induced neuroplasticity

Christine Lucas Tardif [a,*,1], Claudine Joëlle Gauthier [a,b,**,1], Christopher John Steele [a], Pierre-Louis Bazin [a], Andreas Schäfer [c], Alexander Schaefer [d], Robert Turner [c], Arno Villringer [a]

[a] Department of Neurology, Max Planck Institute for Human Cognitive and Brain Sciences, Leipzig, Germany
[b] PERFORM Centre/Department of Physics, Concordia University, Montreal, Canada
[c] Department of Neurophysics, Max Planck Institute for Human Cognitive and Brain Sciences, Leipzig, Germany
[d] Department of Electrical and Computer Engineering, Clinical Imaging Research Centre & Singapore Insitute for Neurotechnology, National University of Singapore, Singapore

ARTICLE INFO

Article history:
Accepted 20 August 2015
Available online 28 August 2015

Keywords:
Brain plasticity
Learning
Quantitative MRI
Multi-modal MRI

ABSTRACT

Over the last two decades, numerous human MRI studies of neuroplasticity have shown compelling evidence for extensive and rapid experience-induced brain plasticity in vivo. To date, most of these studies have consisted of simply detecting a difference in structural or functional images with little concern for their lack of biological specificity. Recent reviews and public debates have stressed the need for advanced imaging techniques to gain a better understanding of the nature of these differences – characterizing their extent in time and space, their underlying biological and network dynamics.

The purpose of this article is to give an overview of advanced imaging techniques for an audience of cognitive neuroscientists that can assist them in the design and interpretation of future MRI studies of neuroplasticity. The review encompasses MRI methods that probe the morphology, microstructure, function, and connectivity of the brain with improved specificity. We underline the possible physiological underpinnings of these techniques and their recent applications within the framework of learning- and experience-induced plasticity in healthy adults. Finally, we discuss the advantages of a multi-modal approach to gain a more nuanced and comprehensive description of the process of learning.

Introduction

It is well accepted that the brain is plastic, having the lifelong capacity to alter its structure and function as a mechanism for healthy development, learning, memory, and recovery from brain injury and disease. Much of what we know about the complex underlying (sub-) cellular mechanisms has been gained from animal models. Candidate mechanisms at the neuronal level include long-term potentiation and depression (LTP, LTD) (Rioult-Pedotti et al., 2000), synaptogenesis (Xu et al., 2009), neurogenesis (Gould et al., 1999), and changes in neuronal morphology (Lerch et al., 2011; Tronel et al., 2010). While these neuronal mechanisms have received much attention (Holtmaat and Svoboda, 2009), restructuring of non-neuronal tissue components has also been shown to occur, e.g. angiogenesis (Black et al., 1991; Kerr et al., 2010) as well as changes in glial cell morphology and density (Dong and Greenough, 2004). In fact, astrocytes (Theodosis et al., 2008), microglia (Kettenmann et al., 2013), oligodendrocytes, and the myelin they produce (Fields, 2010; Gibson et al., 2014; Haroutunian et al., 2014) may play a larger role than previously thought. While these important and biologically specific findings on the plasticity process were gained by invasive methods such as histology, immunohistochemistry, electron and multi-photon microscopy, these methods are not suitable for in vivo human investigations. Furthermore, these techniques can only offer a local snapshot in time of these complex processes, and thus cannot easily be used to study systemic effects.

In vivo magnetic resonance imaging (MRI), on the other hand, gives us the big picture: it enables non-invasive longitudinal investigation of the entire brain. MRI depicts complex patterns of change in space and time, which can be correlated with measures of behavior, performance, or training. In the last decade, MRI has proven to be a valuable tool to study neuroplasticity from a complementary angle to invasive studies on animal models. Imaging studies have shown compelling evidence for extensive and rapid brain plasticity in humans in vivo, starting with seminal cross-sectional studies that showed enlargement of the corpus callosum in professional musicians (Schlaug et al., 1995) and of the hippocampi of London taxi drivers (Maguire et al., 2000). Subsequent longitudinal MRI studies have shown evidence for learning-

* Correspondence to: C.L. Tardif, Max Planck Institute for Human Cognitive and Brain Sciences, Stephanstrasse 1A, 04103 Leipzig, Germany.
** Correspondence to: C. J. Gauthier, Department of Physics, Concordia University, Richard J. Renaud Science Complex, 7141 Sherbrooke West, Montreal, Canada.
E-mail addresses: ctardif@cbs.mpg.de (C.L. Tardif), claudine.gauthier@concordia.ca (C.J. Gauthier).
[1] The first two authors contributed equally to the manuscript.

http://dx.doi.org/10.1016/j.neuroimage.2015.08.047
1053-8119/

induced gray matter structural plasticity (Draganski et al., 2004), and have raised the possibility that individual brain structure can be used to predict subsequent performance and plasticity (Gryga et al., 2012; Sampaio-Baptista et al., 2014; Supekar et al., 2013; Voss and Zatorre, 2012). More recently, white matter structural changes have been characterized with diffusion tensor imaging (DTI) in cross-sectional (e.g. Bengtsson et al., 2005; Johansen-Berg et al., 2007) and longitudinal (e.g. Scholz et al., 2009; Taubert et al., 2010) studies. Evidence for functional remodeling is also extensive, with a number of studies using the blood oxygen level dependent (BOLD) signal to show localized and network-level changes following the course of training (e.g. Albouy et al., 2012; Karni et al., 1995; King et al., 2013; Mackey et al., 2013; Steele and Penhune, 2010). MRI studies on learning-induced and experience-dependent plasticity have made significant contributions to our understanding of the characteristic spatial and temporal patterns of structural and functional brain changes at the macroscopic level, yet their biological interpretation is uncertain. Interpretation of MRI signals is not straightforward, as they tend to be indirect measures of the phenomena we wish to study, and the attribution of MR contrasts to purely structure or function is a simplification since all contrasts are sensitive to some aspects of both.

A number of reviews have summarized the contributions of MRI to the field of learning- and experience-induced neuroplasticity (Draganski and May, 2008; Lövdén et al., 2010a; May, 2011; Voelcker-Rehage and Niemann, 2013), with a focus on the dynamics of structural MR changes in motor learning (Dayan and Cohen, 2011; Taubert et al., 2012), physical activity and exercise (Erickson et al., 2012; Voss et al., 2013), underlying cellular mechanisms (Zatorre et al., 2012), methodological limitations (Lövdén et al., 2013; Thomas and Baker, 2013), and the need for quantitative microstructural characterization using MRI (Draganski et al., 2014). These reviews highlight that MRI studies of structural neuroplasticity have mainly consisted of detecting change in a single qualitative structural MRI contrast (for GM) and diffusion tensor imaging (for WM) using uni-modal voxel-based morphometry (or similar techniques). These methodologies provide limited insight into the underlying neurobiological processes that mediate the macroscopic morphological effects of plasticity. Since there is not a one-to-one mapping between these MR contrasts and underlying biology, structural changes cannot be interpreted readily (as illustrated in Fig. 1). Animal studies using a combination of MRI and histology can be used to create models of plasticity which can help interpret the MR changes observed in humans in vivo (Blumenfeld-Katzir et al., 2011; Lerch et al., 2011; Pereira et al., 2007; Sagi et al., 2012; Sampaio-Baptista et al., 2013). However, this approach makes it problematic to study advanced cognitive tasks and is subject to the interpretation limitations of animal models. There is an emerging consensus that the field of neuroplasticity research would greatly benefit from MR imaging methods that are more biologically specific—methods that can help bridge the gap between the macroscopic systems-level view and the underlying cellular and molecular mechanisms.

One of the main strengths of MRI is its versatility. We can generate multiple complementary image contrasts that probe different characteristics of brain tissue microstructure and function. This versatility has so far been under-exploited and studies have often focused on a single contrast. Furthermore, instead of qualitative images, quantitative maps of the tissue's magnetic resonance properties can be measured. Quantitative images are more straightforward to interpret in terms of underlying biology and eliminate many methodological biases (e.g. sensitivity to field inhomogeneities) that are not relevant to the tissue, thus improving reproducibility across studies and sites.

This article reviews current advanced MRI techniques and suggests how they could be used to further our understanding of learning- and experience-induced brain plasticity in humans in vivo. This is not a comprehensive review of MRI techniques; it is rather a collection of those that seem promising for the study of neuroplasticity. While it is currently premature to provide the readers with a narrow set of techniques, our goal is to lay the groundwork for in vivo MRI-based characterization of neuroplasticity by providing more information about the relevant techniques and their interpretations. We will focus on the biological underpinnings of these imaging techniques within the framework of learning- and experience-induced changes in healthy adults and discuss recent applications from the literature wherever possible. We will argue for a multidisciplinary approach, combining biological science and neuroimaging, to gain a more comprehensive view on plasticity.

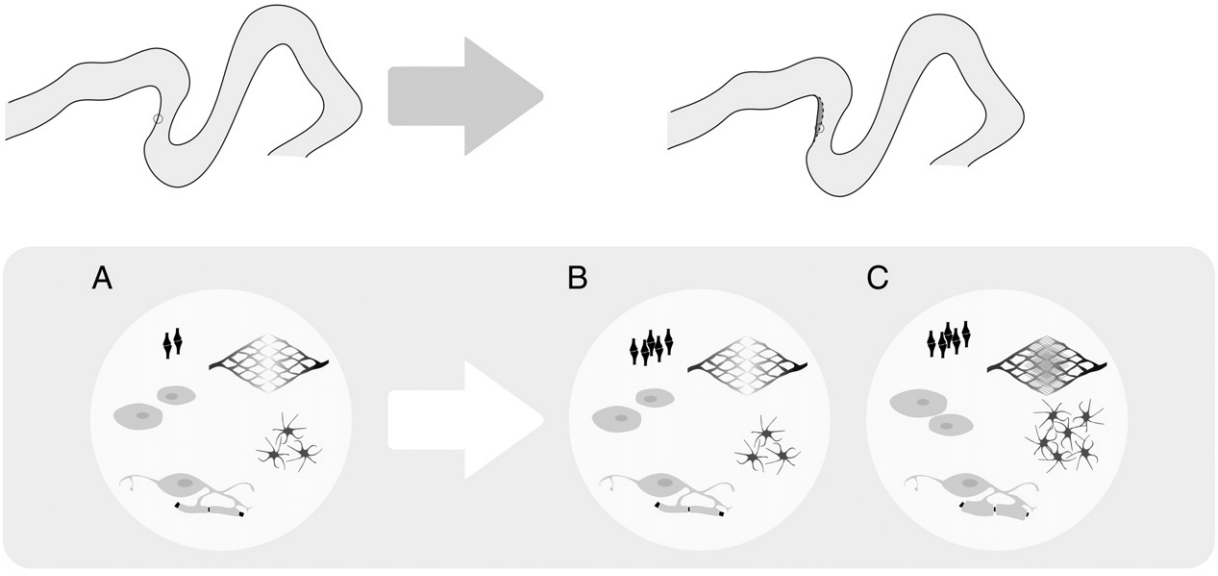

Fig. 1. Schematic of the complex mapping between an MR measure, here cortical thickness, and the underlying biological mechanisms of plasticity. The baseline state is represented in A. Early MRI studies interpreted a change in cortical thickness to be caused by synaptogenesis, represented in B. However, synaptogenesis most likely does not occur in isolation. C is a more realistic representation of the multiple cellular mechanisms at play and that could contribute to a change in cortical thickness. For instance, changes in myelination (increase in myelin sheath thickness or the creation of new myelin sheaths) may occur in the white and gray matter. Both synaptogenesis and myelination require an increase in blood supply (whether a transient increase in blood flow and volume or angiogenesis). Astrocytes will most likely swell as they are targeted to provide the additional nutrients. Cellular density (mainly glial cells but also neurons in the hippocampus) will also most likely increase.

Structural MRI

In 1962, Rosenzweig and colleagues made an unanticipated finding that shaped the field of brain plasticity research: "The finding that cortical weight increases as a consequence of experienced enriched environment." (Rosenzweig et al., 1962) As methodology improved, the field moved on to study the anatomical changes at the microscopic level, mainly morphological changes in synapses and dendrites that underlie these macroscopic effects. Forty years later with MRI, similar to the findings of Rosenzweig and colleagues, macroscopic changes in gray matter morphology were identified in humans in vivo after a 3-month intervention of learning to juggle (Draganski et al., 2004).

In 1949, Hebb postulated that when a neuron repeatedly takes part in the activation of another neuron, the efficacy of the connections between these neurons is increased (Hebb, 1949). Since Hebb's initial theory on synaptic plasticity (both functional and structural) as a mechanism for the adaptation of neurons during learning, research has mainly focused on the role of the synapse as a mechanism for learning. The potential contribution of WM to plasticity has been somewhat neglected. Even so, an early cross-sectional MRI study of musicians suggested that use-dependent brain plasticity could be represented by an increase in size of the corpus callosum (Schlaug et al., 1995). A decade later, Bengtsson et al. used DTI to show the impact of extensive practice on WM development (Bengtsson et al., 2005). Several cross-sectional and longitudinal studies have since shown structural WM plasticity for a variety of tasks (e.g. Lövdén et al., 2010b; Scholz et al., 2009; Taubert et al., 2010; Valkanova et al., 2014).

Though MRI studies have made significant contributions to our understanding of plasticity in humans, limitations in the methodologies that are conventionally used have cast doubt on the results from previous neuroimaging studies of brain plasticity, as illustrated by the debate initiated by Thomas and Baker (2013) and the review by Lövdén et al. (2013). Changes in gray matter density, volume, and thickness have been observed following learning using morphometric analyses of T1-weighted data, typically at 1 mm isotropic resolution. The non-quantitative nature of T1-weighted contrast makes it sensitive to many confounds that are not specific to the underlying biology; for instance, the inhomogeneity of the transmission field, different field strengths, scanning platforms and coils, and minor changes in the post-processing protocols. These confounds reduce the reproducibility of the results and cause biases between different studies and sites.

It remains unclear what the local changes in T1-weighted signal intensity or derived morphological metrics truly reflect at the microscopic scale. Increases or decreases in GM volume and thickness have been postulated to be associated with one or several of the following events: synaptogenesis, spine formation or elimination, dendritic branching or pruning, neurogenesis (mainly in the hippocampus), angiogenesis, gliogenesis, and myelination. Based on the fractional volume of different structures in the cortex (and also within the smallest spatial unit of MRI, a voxel) (see Fig. 2 in Thomas et al., 2012), the complexity of the plasticity process as shown in animal studies, and the MR contrast mechanisms, it is unlikely that a single cellular mechanism leads to the macroscopic changes in brain morphology detected using MRI. DTI metrics, such as fractional anisotropy and mean diffusivity, are also biologically ambiguous and difficult to interpret (discussed in more detail in section 2.1.6). In a recent review, Zatorre et al. illustrate the multiple cellular and molecular mechanisms that could underlie the observed changes in GM morphology and diffusion metrics in the context of learning- and experience-induced plasticity (Zatorre et al., 2012). The authors also discuss the limits of interpretation of current techniques and highlight that it is simply not possible to clearly relate in vivo GM density/volume/thickness or DTI changes to one or several of these biological mechanisms (see Fig. 1).

In the following sections, we will review structural MR imaging and analysis methods that yield more specific and reproducible biomarkers of tissue microstructure than conventional MRI.

Imaging tissue microstructure

The image contrast of MRI relies on different biophysical properties of the tissue: the density of MR visible protons, the relaxation times,

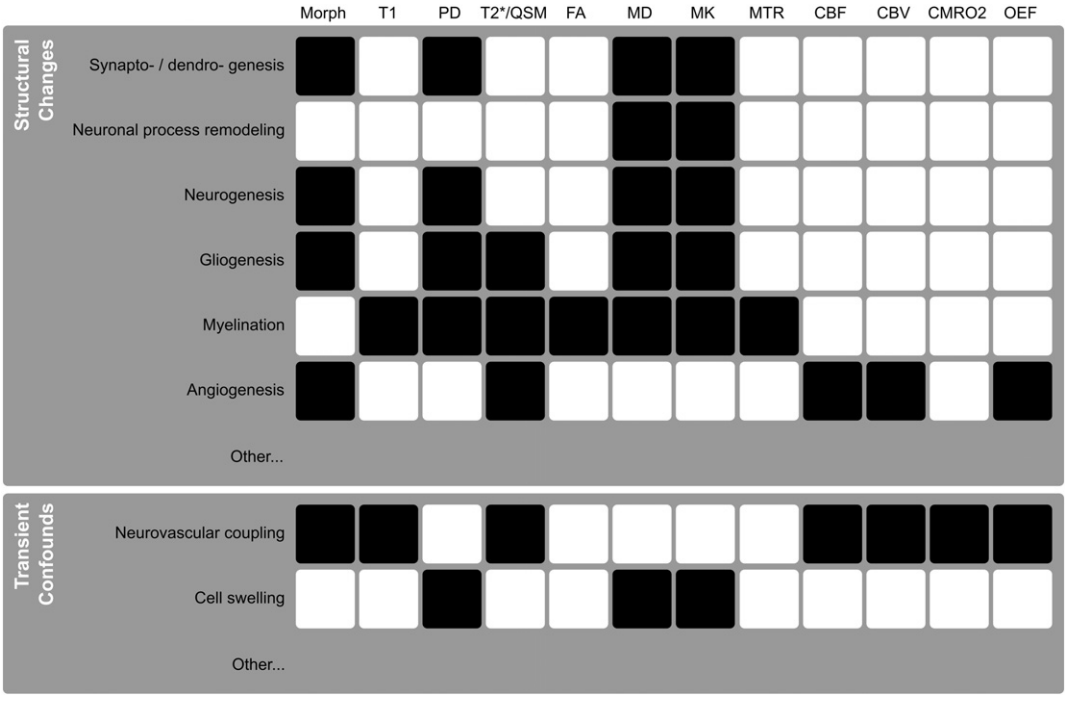

Fig. 2. Diagram illustrating the putative contributions of the different cellular mechanisms of structural plasticity to the different MR contrasts we can measure. The second gray box represents potential transient changes that may act as confounds when trying to detect more permanent structural changes. (Morph: morphometry, PD: proton density, QSM: quantitative susceptibility mapping, FA: fractional anisotropy, MD: mean diffusivity, MK: mean kurtosis, MTR: magnetization transfer ratio, CBF: cerebral blood flow, CBV: cerebral blood volume, CMRO2: cerebral metabolic rate of O_2, OEF: oxygen extraction fraction).

the magnetic susceptibility distribution and magnetization transfer (MT) between macromolecules and water, and the movement of water (diffusion, perfusion). These MR parameters, measured at the macro- to mesoscopic scale (~3 mm to 3 μm), reflect the local environment of magnetic spins (i.e., the tissue microstructure). While various MRI contrasts weigh combinations of these factors differentially (e.g., T1-weighted imaging, T2-weighted imaging, diffusion-weighted imaging etc.), in order to relate MRI findings to underlying physiological and anatomical entities, it is necessary to disentangle their contribution to the MRI signal and to obtain quantitative measures of these factors (quantitative MRI, qMRI). Until recently, quantitative mapping of these parameters was not feasible at high resolution within reasonable scan times. Due to recent hardware improvements, accelerated imaging techniques, and novel MR sequence designs, quantifying these parameters has become practical and accessible to the cognitive neuroscience community.

T1 mapping

The T1 relaxation time characterizes the exponential recovery of the longitudinal magnetization to its equilibrium state. T1 is affected by the interaction of spins with their surrounding lattice. For structured material, such as brain tissue, T1 decreases as the proportion of spins (protons) bound to macromolecules increases (as in brain tissue/GM/WM), whereas T1 increases if more spins are free (as in liquids such as the cerebrospinal fluid (CSF)). Thus, T1 is sensitive to the macromolecular (protein matrices, cell membranes, and large lipids) and water content of brain tissue, and the interaction between the two. In the healthy human brain, T1 mainly reflects variations in myelin content (90% in white matter and 64% in gray matter, although this may vary between brain regions), with a modest contribution from iron (Stüber et al., 2014). Cortical surface representations of T1 or R1 (1/T1) maps have been shown to reflect its myeloarchitecture (Dick et al., 2012; Sereno et al., 2013; Tardif et al., 2015).

The gold standard for T1 mapping is an inversion recovery experiment, where the magnetization is inverted (with a 180-degree pulse) and sampled at several inversion times (TI) during recovery to its equilibrium state (Barral et al., 2010; Mugler and Brookeman, 1990). Several fast T1 mapping techniques have been proposed, at the cost of slight methodological biases (Stikov et al., 2014). A popular fast T1 mapping technique that uses a standard pulse sequence is the variable flip angle (VFA) method, where two or more gradient echo images are acquired using different excitation flip angles while keeping the other parameters constant (Deoni et al., 2005; Fram et al., 1987; Helms et al., 2008). This method is sensitive to inhomogeneity in the $B1^+$ radiofrequency transmission field, and thus a $B1^+$ map should also be acquired at field strengths ≥3 T (for recent reviews of $B1^+$ mapping methods, see Lutti et al., 2010; Pohmann and Scheffler, 2013). It is also crucial to implement an efficient spoiling scheme to accurately estimate T1 (Preibisch and Deichmann, 2009; Yarnykh, 2010). A quantitative extension of the MPRAGE sequence called MP2RAGE was introduced by Marques et al. by including a second gradient-echo readout after a second inversion time (Marques et al., 2010). Using carefully optimized acquisition parameters, the resulting T1 maps are less sensitive to $B1^+$ field inhomogeneity, particularly at 3 T. Whole-brain 1 mm isotropic T1 maps can be acquired in 8 minutes at 3 T using either VFA or MP2RAGE. At 7 T, 0.65 mm isotropic T1 maps can be acquired using the MP2RAGE sequence in 12 minutes. Unfortunately, there is still significant variation in the T1 times reported using different techniques, such that calibration to the gold standard inversion recovery experiment is recommended (Stikov et al., 2014). For a review of high-resolution T1 mapping of the cortex, the readers are referred to Lutti et al. (2013).

Since the main source of T1 contrast in the cortex is myelin, decreased T1 (corresponding to an increase in T1-weighted signal intensity in typical FLASH or MP-RAGE neuroimaging protocols) is likely to reflect an increase in myelination. The importance of the role of subcortical and intra-cortical myelin in normal and pathological brain plasticity throughout the lifespan has gained recognition in recent years (Fields, 2008; Fields et al., 2014; Haroutunian et al., 2014). Intra-cortical myelin plays a key role in optimizing the time and synchrony of action potentials, which is necessary for optimal function of neuronal networks. Subtle adaptive changes in myelination could result in major effects on the rhythmic activity in the brain (Pajevic et al., 2014). A higher degree of intra-cortical myelination in humans, measured in vivo using MRI, has been shown to be associated with greater performance stability across the lifespan during a speeded task (Grydeland et al., 2013). The same group also showed that the degree of myelination of the posterior cingulate cortex was related to the amplitude of a direct electrophysiological measure of neuronal activity (Grydeland et al., 2015). Rodent studies have shown that myelination is responsive to environmental inputs in adults (Liu et al., 2012). During adulthood, progenitor NG2 cells in the brain continue to divide and differentiate, increasing the number of oligodendrocytes by as much as 50% to support continued myelination and remyelination (Peters, 2009). In vitro studies have shown that electrical activity in axons promotes myelination after only a few hours (Wake et al., 2011) and has an effect on oligodendrocyte development and differentiation into myelinating glia (Stevens et al., 2002). Furthermore, a recent in vivo study in mice showed that neuronal activity drives oligodendrocyte precursor cells to proliferate, migrate, and make contact with axons, and then differentiate into mature oligodendrocytes to generate myelin (Gibson et al., 2014). The addition of new myelin sheaths is mediated by newly differentiated oligodendrocytes within a critical period, which may be as rapid as 5 hours (Czopka et al., 2013). In addition to myelinating naked axons, Young et al. showed that adult-generated oligodendrocytes actively remodel the thickness of existing myelin sheaths to fine tune the speed of action potentials (Young et al., 2013), modulating the long-range synchronization of signals. Myelin also plays a stabilizing role in structural plasticity, with myelin associated growth inhibitors limiting activity, experience-induced axon sprouting, and synaptic plasticity (Akbik et al., 2012). Myelination is the dominant source of T1 contrast in the brain, particularly in the cortex; however, other microstructural features that are independent of the myelin volume fraction, notably axon diameter, also affect T1 (Harkins et al., 2015) and could change during learning (Zatorre et al., 2012). A general linear model of R1 (1/T1) that describes its dependence on macromolecules, iron, and water content has been proposed (Callaghan et al., 2015).

Differences in T1 are not solely attributable to changes in underlying microstructure. As with most sources of MR contrast, T1 is at the intersection of structure and function. Changes in T1 may stem partly from changes in cellular density (see section 1.1.2), functional or physiological source (see Fig. 2). It is possible that transient physiological changes in blood volume, flow, or dissolved oxygen, or more permanent changes from angiogenesis could cause the signal change observed. For example, oligodendrocyte precursor cells have very high metabolic requirements as they differentiate to produce myelin segments and must first secure better access to the blood supply (Yuen et al., 2014). An increase in dissolved oxygen has been shown to decrease cortical T1 values by up to 0.5% in comparison to air while breathing 100% oxygen (Haddock et al., 2013). On the other hand, changes in the size of the vascular bed (and therefore its relative contribution to the voxel signal) could counteract this effect since the T1 of blood is higher than the T1 of brain tissue (Lu et al., 2003). An increase in blood volume could also lead to an increase in local tissue volume, which will affect local measures of GM volume and thickness.

Water and macromolecular tissue volume

Proton density (PD) maps are a reliable quantitative estimate of the free water content (or the complementary macromolecular content) of

brain tissue (Tofts, 2003). There is a strong linear relationship between T1 and PD in brain tissue. Both parameters are affected by variations in the density of neurons, synapses, and glial cells, for instance, which may increase or decrease (e.g. cell and synaptic pruning) during plasticity. Deviations from the linear relationship could provide information with respect to changes in the local physico-chemical environment. For instance, T1 is differentially affected by the cholesterol of the myelin sheath and iron. The macromolecules within brain tissue are principally in cell membranes and proteins. In white matter, approximately 50% of macromolecules constitute the myelin sheaths.

The VFA spoiled gradient echo protocol, described above for T1 mapping, can also be used to simultaneously measure free water content or macromolecular tissue volume (MTV) (Deoni et al., 2005; Mezer et al., 2013). Using CSF as a reference for 100% water, the amount of water within a voxel can be estimated from the PD signal and the residual portion of the voxel is equal to the MTV fraction. Following this calculation, PD and MTV maps must be corrected for spatial variation in the sensitivity of the $B1^-$ RF reception field. Recently, simple and robust methods for unbiased measurements of MTV and its complementary free water volume using standard pulse sequences at different field strengths have been proposed (Abbas et al., 2015; Mezer et al., 2013; Volz et al., 2012).

T2, phase and magnetic susceptibility mapping*

Conversely to T1, the T2* relaxation time describes the decay of the magnetization that has been tipped into the transverse plane. T2* is influenced by the spin–spin interaction (T2) and the signal decay due to magnetic field perturbations (T2′). In brain tissue, T2* is used to assess iron, myelin, and deoxyhemoglobin content (blood oxygenation—see section 3.2) (see Chavhan et al., 2008 for a review). In the cerebral cortex, iron is co-localized with myelin in the normal brain because oligodendrocytes have the highest iron content of all brain cell types. Iron is localized in the soma of oligodendrocytes and is necessary for their differentiation (Todorich et al., 2009, 2011). 7 T T2* maps of the cortex have been shown to reflect its myeloarchitecture (Cohen-Adad et al., 2012).

A multi-echo spoiled gradient echo sequence can be used to sample the T2* signal decay and calculate a quantitative T2* map. In addition to the magnitude signal, gradient echo imaging can be used to produce a phase image, which corresponds to the angle between the imaginary and the real parts of the complex MR image. The phase images display the field perturbations that mainly arise from small differences in magnetic susceptibility within the subject's brain in combination with field variations due to inhomogeneities in the static main magnetic field B0. The latter can be removed by applying a high-pass filter such as a homodyne filter (Haacke et al., 2004), sophisticated harmonic artifact reduction for phase data (SHARP) (Schweser et al., 2011; Topfer et al., 2015), or projection onto dipole fields (PDF) (Liu et al., 2011). The filtered phase map reveals excellent contrast between gray and white matter, deep gray matter regions, and is enhanced at higher field strengths (Duyn et al., 2007; Fischl and Wald, 2007). Unfortunately, the phase image itself shows non-local effects and the contrast depends on the orientation of the object to the main magnetic field (Schäfer et al., 2009). To overcome these drawbacks, the local magnetic susceptibility itself can be measured. Several different methods for this technique, termed quantitative susceptibility mapping (QSM), have been developed (Schweser et al., 2013; Wang and Liu, 2015 for a review). A recent study at 7 T compares high-resolution T2* magnitude and phase images to quantitative T2* and susceptibility maps (Deistung et al., 2013b). QSM shows high tissue contrast for the delineation of deep GM structures, and thus shows potential for assessing the microstructure and morphometry of these structures that are difficult to discern in conventional T1-weighted images.

The sources of the T2*, phase, and susceptibility contrast in the human brain are mainly iron and myelin (Fukunaga et al., 2010; Langkammer et al., 2011; Stüber et al., 2014). While both iron and myelin content decrease T2*, in QSM, it is possible to differentiate between the two due to their different magnetic behavior. Iron is paramagnetic, it has a higher magnetic susceptibility relative to water (i.e., $\chi_p > 0$), whereas myelin is diamagnetic, with a negative magnetic susceptibility (i.e., $\chi_d < 0$). It is now accepted that the magnetic susceptibility anisotropy of myelin and its orientation to the main magnetic field influence the T2* and phase maps within the white matter and the cortex (Cohen-Adad et al., 2012; Lee et al., 2010; Li et al., 2006, 2012; Rudko et al., 2014; Wharton and Bowtell, 2012, 2015). While the generation of new oligodendrocytes (oligogenesis) is accompanied by increased myelination, existing myelin sheaths can also be modulated in response to neuronal activity without the differentiation of oligodendrocyte precursor cells. Similar to T1, changes in physiology (CBF and CBV) could also impact T2* and QSM due to the local concentration of deoxyhemoglobin that increases local magnetic susceptibility, similarly to iron.

While one of the advantages of quantitative imaging is that it can facilitate inter-site and inter-study comparisons, researchers should keep in mind that T1 and T2* relaxation times depend on the magnetic field strength and limit their comparisons accordingly (Koenig et al., 1984; Peters et al., 2007; Rooney et al., 2007). Relaxometry (the measurement of absolute values of T1, T2, or T2* relaxation times) has not, to our knowledge, been used to study learning-induced plasticity, but could be an interesting complementary method to combine with magnetization transfer and/or DWI (see sections 2.1.4 and 2.1.6, respectively) to understand the role of myelin changes. Iron may be more pertinent in disease-related plasticity as it is known to be increased in neurodegenerative diseases.

Incorporating microstructural models

Most relaxometry experiments fit the signal decay or recovery to a mono-exponential curve. However, the relaxation of the magnetization in biological tissues is usually more complex and arises from multiple compartments with different relaxation times. In white matter, the transverse signal decay can be characterized by two T2 components—corresponding to water trapped between the myelin bilayers (T2 < 50 ms) and the intra-/extra-cellular water pools (T2 > 70 ms) (MacKay et al., 1994). The ratio of the myelin water to the total water is termed the myelin water fraction (MWF). Multi-component relaxometry techniques, recently reviewed in Alonso-Ortiz et al. (2015), are more specific than single component relaxometry but also more limited in terms of spatial resolution and coverage.

Another technique that is also more specific to myelin content is magnetization transfer (MT) imaging. With MT, it is possible to indirectly image the macromolecules, e.g. proteins and lipids, which have a T2 that is too short to be directly detected with MRI. The macromolecular magnetization is saturated using an off-resonance RF pulse, the macromolecules transfer their magnetization to the water protons, resulting in a decrease in MR signal (Henkelman et al., 2001). Recent studies have modified the MT pulse sequence to lower the specific absorption rate, a limiting factor especially at ultra-high field (Dortch et al., 2013; Mougin et al., 2010). Most often, the MT ratio (MTR) is calculated between the original and MT-saturated images (Wolff and Balaban, 1989). MTR is a semi-quantitative measure dependent on the imaging protocol and presents only a limited view of the MT effect (Portnoy and Stanisz, 2007). On the other hand, high-resolution MTR images correlate with myelin content in both WM and GM (Schmierer et al., 2008, 2010) and can be acquired in reasonable scan times. Contrarily to MTR, MT saturation (MT_{SAT}) accounts for spatial variations in the RF field and T1 (Helms et al., 2010), resulting in higher brain tissue contrast that is more specific to myelination (Callaghan et al., 2015).

A recent study of early blind individuals in comparison to late blind and sighted individuals showed bidirectional changes in MTR in different visual areas, mainly located at white/gray matter boundaries (Voss et al., 2014). An increase in MTR could reflect increased myelination

(due to a higher density of myelinated axons or increased myelin thickness) or increased cellular density. A more complete characterization could be performed using a quantitative MT protocol and a two-pool tissue model (Henkelman et al., 2001; Sled and Pike, 2001) at the cost of scan time, resolution, and coverage. The two-pool model can be further extended to model the different myelin water compartments (Levesque and Pike, 2009). A recent study has shown that, similarly to T2*, magnetization transfer parameters are also sensitive to the orientation of the myelinated fibers to the main magnetic field B0 (Pampel et al., 2015).

The bound pool fraction (of the two-pool qMT model) and MWF are highly correlated with MTV in brain tissue (Mezer et al., 2013). Due to the limited SNR efficiency of the former techniques, they are impractical for in vivo imaging studies of plasticity where subtle local changes in tissue microstructure occur. MTV and MTR, on the other hand, may be more suitable for detecting subtle local changes in microstructure distributed over the brain due to learning.

Efficient multi-parametric structural mapping

Some of the above MR parameters may be measured together in a more efficient way. For instance, T1 and PD can be measured in a single scan, with the addition of an additional scan to map receive field non-uniformity. T2*, phase, and susceptibility maps can all be extracted from a multi-echo gradient echo protocol. Recently, a multi-echo implementation of the MP2RAGE sequence was proposed to measure T1, T2*, and QSM from a single acquisition (Metere et al., 2015). A multi-parametric approach combining T1, T2*, MTR (or MT_{SAT}), and PD introduced by (Helms et al., 2008) has successfully been implemented in a multi-center study (Weiskopf et al., 2013b). This protocol yields whole-brain 1 mm isotropic parametric maps in ~19 minutes. Another advantage of multi-parametric mapping techniques is that the same field of view, resolution, and readout schemes are used, resulting in the intrinsic alignment of the resulting maps. As discussed in more detail in section 5, multi-modal MRI will play an important role in narrowing down the biological mechanisms underpinning plasticity.

Diffusion-weighted imaging

Diffusion-weighted imaging (DWI) is currently the only method capable of mapping fiber architecture in the living human brain and has proven to be a useful technique for probing brain tissue microstructure. Critical reviews of the potential and pitfalls of DWI are presented in Concha (2013) and Jones et al. (2013).

DWI measures the dephasing of spins in the presence of a spatially varying magnetic field (a gradient) due to incoherent displacement of the spins along the axis of the gradient. The loss of signal coherence results in a signal reduction in comparison to a non-diffusion encoded acquisition. In highly organized and coherent microstructure, water diffusion follows a preferred direction, e.g. along the fiber. The diffusion propagator of the water molecules can be sampled using multiple MRI acquisitions where the diffusion dephasing is measured along different directions and for different diffusion-weightings (b-values or shells). This information is then used to reconstruct continuous long-range trajectories from local estimates of fiber orientation, a method known as tractography (Mori et al., 2002; Tournier et al., 2011). The random displacement of water molecules can be impeded by many factors including, but not limited to, fiber diameter, fiber density, membrane permeability, myelination, and intra-voxel orientational coherence of any boundaries (Beaulieu, 2002).

Diffusion tensor imaging. The most commonly used model to characterize the geometry of the diffusion propagator is the tensor. The tensor model in diffusion tensor imaging (DTI) can be used to calculate voxel-based scalar measures, including mean diffusivity (MD), radial and axial diffusivity (RD and AD), and fractional anisotropy (FA) (Basser, 1995; Song et al., 2002). DTI requires a minimum of 6 unique directions to estimate the diffusion tensor, but 30–60 directions are recommended for more robust estimates (Jones et al., 2013). Using the current state-of-the-art in hardware and acquisition techniques, a 2.5–1.5 mm isotropic diffusion data set with 60 directions can be acquired within 15–30 minutes at 3 T. The tensor metrics, such as FA, are commonly analyzed throughout the brain with voxel-based and skeletonized (Smith et al., 2006) approaches. In the latter, the WM fiber organization is approximated with a groupwise skeleton onto which subject-specific maps are projected for analysis. Other methods have been investigated to take into account individual fiber tracts (Bazin et al., 2011; Corouge et al., 2006; O'Donnell et al., 2009), which can then be used as ROIs or to constrain voxel-based analyses (Cercignani, 2010; Lebel et al., 2008). It is also possible to analyze DTI data using a bi-tensor model to differentiate the contribution of the free water compartment (including CSF and extracellular space) from the tissue compartment (Pasternak et al., 2009). Free water imaging will generate DTI metrics that are more specific to the tissue in voxels at the boundary of the WM with the ventricles and at the cortical surface that contain partial volume effects with CSF. Free water maps and corrected DTI metrics have also been applied to patients to assess the role of neuroinflammation (Pasternak et al., 2012).

DTI has greatly contributed to the study of subtle differences in tissue microstructure. FA has been widely used to assess the relationship between WM structure and behavior in humans (Johansen-Berg, 2010) and has recently been applied in an effort to quantify WM plasticity (see Zatorre et al., 2012; for a review, Scholz et al., 2009; Steele et al., 2013; Taubert et al., 2010). Increases in FA are typically observed in association with maturation, development, or learning (Scholz et al., 2009). However, reduced FA has also been observed (Taubert et al., 2010) and could be attributed to an increase in axon diameter or the maturation of a secondary fiber population in a region of fiber crossing. Hofstetter et al. performed a similar motor learning study in rats and humans and found a decrease in FA, AD, and MD in the fornix of both species (Hofstetter et al., 2013). In two other animal studies, an increase in FA of the corpus callosum (Blumenfeld-Katzir et al., 2011) and in the WM of the sensorimotor cortex (Sampaio-Baptista et al., 2013) coincided with an increase in myelination detected using immunohistochemistry. Whereas in the first case, a hippocampal-dependent spatial navigation task in a water maze was performed and could have elicited new neurons to establish new efferent connections, in the second study by Sampaio et al., a cortical learning paradigm (reaching training) was used during which neurogenesis is unlikely to occur. Both studies reported an increase in FA and myelin basic protein expression; however, they did not find any correlations between the two measures, hinting that FA is likely sensitive to multiple cellular mechanisms in addition to myelination.

Several DTI studies have shown a decrease in MD in the GM, in particular in the hippocampus, due to learning in animals (Blumenfeld-Katzir et al., 2011; Ding et al., 2013; Sagi et al., 2012; Sampaio-Baptista et al., 2013; Scholz et al., 2014). Similar to the WM plasticity study by (Hofstetter et al., 2013), Sagi et al. performed a particularly interesting study combining DTI in animals and humans in the hippocampus (Sagi et al., 2012). The authors suggest that the decrease in MD may reflect an overall shift in the ratio of extracellular to intracellular space. The two studies by Sagi et al. (2012) and Hofstetter et al. (2013), which use the same spatial learning task (and overlapping data sets), show that learning can induce rapid structural plasticity, after only 2 hours of training in the hippocampus of humans and rats, and after 2 hours and 1 day of training in the fornix of humans and rats, respectively. Furthermore, the structural changes in WM and GM are linked, although we do not know the directionality of the underlying mechanisms.

Complex fiber geometries. The actual meaning of tensor-derived metrics (MD and FA) is ambiguous. The tensor assumes unidirectional diffusion and thus poorly reflects underlying tissue organization when fibers are not uniformly aligned (such as is the case with crossing, kissing, and

fanning fibers). Since it is estimated that 63–90% of voxels in the human brain contain crossing fibers, it is clear that diffusion tensor-derived metrics are not physiologically specific (Jones et al., 2013). A number of techniques have recently been developed to provide more specific and anatomically relevant metrics of white-matter anatomy. Diffusion models that are better able to handle complex fiber architectures, such as the fiber orientation density function calculated with constrained spherical deconvolution (CSD) (Tournier et al., 2007), can be paired with probabilistic tract tracing techniques to produce anatomically plausible tractography (Girard et al., 2014). Tract-density imaging (TDI) can be used to produce super-resolution images that are strikingly consistent with known anatomy (Calamante et al., 2011; Deistung et al., 2013a).

Resolution is important in many MR modalities to increase sensitivity to subtle local changes. In DWI, high-resolution is particularly crucial to minimize the impact of complex fiber geometries within a voxel, which could otherwise conceal changes in individual tracts. For instance, there are U-fibers and subcortical WM tracts near the WM/GM tissue boundary that make sharp turns to enter the cortex. Image acquisition techniques that provide higher resolution, up to 800 μm at 7 T, in combination with constrained spherical deconvolution, have shown these subcortical fiber geometries (Heidemann et al., 2012). An interesting multi-contrast approach to tractography combines DWI with high-resolution T2*-weighted gradient echo images which are sensitive to susceptibility differences between fiber bundles and to the orientation of the fiber bundles to the main magnetic field B0 (Kleinnijenhuis et al., 2012). The high-resolution T2* data can guide the tractography in areas of complex fiber geometries that are difficult to resolve using typical DWI resolutions.

Microstructural models. These more complex diffusion models and fiber reconstruction algorithms have contributed important qualitative descriptions of brain connectivity. In the context of plasticity, we are interested in quantifying tract properties that may change due to learning or experience. Voxel- and tract-based measures derived from these advanced diffusion models and that are specific to a fiber bundle, such as streamline density or spread, have been used to characterize the "strength of connection" of white matter tracts (Dell'Acqua et al., 2013; Raffelt et al., 2012; Riffert et al., 2014; Sotiropoulos et al., 2012). These metrics can be compared between groups or across time with methods such as plausibility tracking (Schreiber et al., 2014). Yet, several authors have discussed the pitfalls of common terminology and urged users to interpret their results cautiously (Jones and Cercignani, 2010; Jones et al., 2013). In particular, streamline density is not equivalent to fiber density. Due to methodological limitations, tractography results are sensitive to the topology of the fiber tract, which may vary between subjects. While these methods provide the opportunity to quantify plasticity occurring along specific fiber tracts in longitudinal studies, users should be skeptical of using them in a cross-sectional study design.

In addition to its inability to account for complex fiber geometry, the diffusion tensor model is also a limited characterization of tissue microstructure due to the use of a single shell (b-value) and the assumption of anisotropic Gaussian diffusion. Thus, the model does not allow for multiple compartments with different diffusion metrics or restricted diffusion within the axons. Because of this, a difference in FA could be caused by an underlying difference in myelination, axon diameter, packing density, or membrane permeability (Beaulieu, 2002). Since neurons and glia are tightly coupled, it is likely that several of these changes occur together. For example, myelination is regulated by axon diameter. Therefore, a change in axon diameter during learning could in turn cause oligodendrocytes to alter the thickness of myelin sheaths. Conversely, oligodendrocytes can regulate axon diameter and even the survival of axons. All we can say is that a change in FA means that some orientation-dependent aspects of the microstructure of the tissue are different.

Diffusion kurtosis imaging (DKI), where data are acquired at multiple shells, has been proposed to account for non-Gaussian diffusion (Glenn et al., 2015; Jensen et al., 2005). DKI has been shown to be more sensitive to tissue microstructure and is more appropriate for looking at the GM where the diffusion is more isotropic (Wu and Cheung, 2010). However, acquiring multiple b-values results in either longer acquisition or decreased resolution, which poses its own challenges for investigating changes within the cortex. DKI of a limited field of view at 1.2 mm isotropic resolution at 3 T was performed and showed microstructural differences between cortical areas (Mohammadi et al., 2014). More advanced multi-shell acquisition and analysis schemes based on models of tissue microstructure have been developed to measure more specific microstructural traits, such as axon density, mean axon diameter, and axon diameter distributions (AxCaliber (Assaf et al., 2008), CHARMED (Assaf and Basser, 2005), ActiveAx (Alexander et al., 2010)), as well as neurite orientation dispersion and density imaging (NODDI) (Zhang et al., 2012). AxCaliber, for instance, is based on a diffusion model that includes both restricted (intra-axonal) and hindered (extra-axonal) diffusion to calculate axonal diameter and density (Assaf et al., 2008). Importantly, these tissue parameters have been validated and axon diameter has been linked to inter-individual differences in axon conduction velocity (Horowitz et al., 2015). As highlighted by (Innocenti et al., 2015), these methods are biased toward large axons since they fail to resolve axons in the 1–2 μm range. Temporal diffusion spectroscopy uses oscillating instead of bipolar diffusion sensitizing gradients to achieve significantly shorter diffusion times (Parsons et al., 2006). Recently, this novel technique has been used to quantify cell size (including axon diameters <2 μm) and intracellular volume fraction (Jiang et al., 2015; Xu et al., 2014).

Quantifying changes in brain shape and size

To date, MRI has mostly been used in the field of learning- and experience-induced plasticity to detect differences in the morphology (volume, density/probability, and shape) of brain structures. Typically, T1-weighted images with optimal contrast-to-noise ratio between GM, WM, and cerebrospinal fluid (CSF) are acquired in order to perform automated tissue classification. The images are analyzed using tools such as voxel-based morphometry (VBM), a whole-brain voxel-based statistical analysis technique that detects local differences in GM (density, probability, or volume) once gross anatomical differences have been accounted for by registration to an atlas (Ashburner and Friston, 2000). This established and straightforward technique is freely available via many software packages, including SPM, FreeSurfer, and FSL, and has been extensively used to detect subtle yet consistent learning- and experience-induced changes in GM morphology.

To be accurate, VBM methods must incorporate high-precision inter-subject registration (Klein et al., 2009), meaningful modeling of the deformations as diffeomorphisms (Miller, 2004), and reliable structure segmentation and tissue estimation. In the brain, the structural variability of the cerebral cortex makes all these steps challenging to perform at the level of precision required to measure small anatomical changes at the macroscopic scale. Although the VBM approach has been under debate for many years (Bookstein, 2001; Davatzikos, 2004; Thompson and Holland, 2011), it is prevalent in existing plasticity studies.

It is not clear whether VBM changes reflect changes in brain morphology, brain microstructure (i.e. a local change in GM signal but not in the position of the true anatomical boundary), or a combination of both (Lövdén et al., 2013). Furthermore, VBM results may depend strongly on the choice of spatial smoothing kernel used (e.g. Jones 2005), and such mandatory smoothing itself strikingly reduces the spatial specificity of this technique. Thus, it may be impossible to distinguish changes in gray matter density across the banks of a sulcus. In contrast to VBM, deformation-based morphometry (DBM) focuses on

statistics of the deformations themselves, which are more easily interpretable as local changes in the boundaries between tissues (Davatzikos et al., 2001). DBM can either be applied to the whole brain or to segmented structures of interest. It is particularly adapted to longitudinal analyses, where the deformations are almost exclusively driven by the true underlying structural changes we wish to measure. Recent work in mice has demonstrated the benefit of using deformations together with high-resolution imaging to detect changes in small structures (Cahill et al., 2015). In addition to animal studies (Lerch et al., 2011; Scholz et al., 2014, 2015), DBM has also been applied to measure structural change in children undergoing 15 months of musical training (Hyde et al., 2009). New methods for shape analysis and statistics on deformations (Ng et al., 2011; Younes, 2010; Baloch and Davatzikos, 2009) are emerging, but still difficult to apply cross-sectionally on complex shapes such as the cerebral cortex or multi-shape ensembles such as a detailed segmentation of the whole brain, and non-trivial biases can still arise (Yushkevich et al., 2010).

Scalar measures of local structure and shape that do not depend on tissue densities/probabilities/memberships are possible. Cortical thickness has been shown to be a more sensitive measure in certain circumstances (Hutton et al., 2009) and is widely used, although it still suffers from variability based on the underlying segmentation procedure, image contrast, or resolution (Lüsebrink et al., 2013). Other cortical measures can be derived such as gyrification, cortical surface area, and sulcal depth (Gautam et al., 2015; Tosun et al., 2011), though some of these measures may be more pertinent for neurodevelopment research rather than training-induced plasticity. However, these measures focus exclusively on the cerebral cortex, ignoring key structures involved in learning such as the hippocampus and the cerebellum. For the hippocampus and other structures with a relatively simple geometry, changes can be measured via shape descriptor analysis (Das et al., 2012; Dill et al., 2015; Gerardin et al., 2009; Voineskos et al., 2015). The cerebellum is more challenging to segment and measure, due to its complexity of shape and small size (Bogovic et al., 2013; Diedrichsen et al., 2009; Park et al., 2014).

The quantitative MR imaging contrasts outlined above have the potential to drastically improve the VBM methodology in several ways. Because quantitative T1 and MT are more directly linked to myelin content alone than T1-weighted images, they also provide a more reliable basis for segmenting the brain and estimating cortical thickness or tissue densities (Draganski et al., 2014; Weiskopf et al., 2013a), and adapted segmentation algorithms are emerging (Bazin et al., 2014; Fujimoto et al., 2014; West et al., 2012). The impact of field inhomogeneities is greatly reduced in quantitative MRI, leading to reduced variability in the segmentations. Furthermore, smaller subcortical nuclei can be better imaged and segmented with a combination of quantitative contrasts such as MT and QSM (Helms et al., 2009; Keuken et al., 2014; Lenglet et al., 2012). Multiparametric quantitative or semi-quantitative measures can also help improve the co-registration of cortical areas within and across subjects (Frost and Goebel, 2013; Robinson et al., 2014; Tardif et al., 2015), reducing or even removing the need for data smoothing and thus increasing precision and the sensitivity to focal change (Turner, 2014).

Going beyond GM density/volume/thickness

There are two partially independent measures of structural plasticity that contribute to T1-weighted GM density/probability measured using VBM: changes in local volume and local tissue microstructure (Lövdén et al., 2013). Using advanced MRI techniques, we can get a more specific characterization of plasticity-related changes by better isolating these effects. We can achieve more precise measures of brain morphology by using image contrasts that are minimally sensitive to methodological confounds such as B1. As discussed above, T1 maps are an excellent candidate. Alternatively, T1-weighted/T2-weighted (Ganzetti et al., 2014; Glasser and Van Essen, 2011) or T1-weighted/PD-weighted (Van de Moortele et al., 2009) image ratios can also be used. Further, DBM and high-resolution imaging could improve the sensitivity to and precision of the morphological differences.

Multiple complementary image contrasts can be combined to create a more specific marker of the microstructural changes that occur within the GM. MTV can be used to measure a change in macromolecules (cellular membranes and proteins). T1 could help determine whether the increase in MTV is due to an increase in the proportion of cholesterol found in myelin sheaths (Mezer et al., 2013). T2* and QSM could be acquired to differentiate changes in myelination from changes in oligodendrocyte density. We would recommend using one of the multiparametric mapping protocols described in section 2.1.5.

DTI and DKI of the GM could also give complementary information to T1. A decrease in mean diffusivity could be due to a shift from extra- to intracellular space due to cell swelling or increased cellular density, the underlying mechanisms of which would depend on when in the time course of plasticity this change is measured (Johansen-Berg et al., 2012). An increase in mean kurtosis would reflect non-gaussian diffusion due to the enhanced restriction of membranes. Kurtosis metrics could be sensitive to the remodeling of neuronal and glial processes, including genesis and pruning, which may impact T1 to a lesser extent. Changes in the kurtosis tensor could give us information on the orientation in which these changes take place.

T1 has also been shown to vary as a function of axon diameter in the WM (Harkins et al., 2015). Furthermore, myelination and axon diameter are tightly coupled in the brain. Change in axon diameter during learning could cause oligodendrocytes to alter the thickness of the myelin sheath, and conversely, oligodendrocytes can regulate axon diameter and survival (Zatorre et al., 2012). It would thus be interesting to acquire an independent diffusion-based MRI measure of axon diameter (Assaf et al., 2008) as discussed in section 2.1.6. Furthermore, the myelin g-ratio, the ratio between the inner and the outer radius of the myelin sheath that envelops an axon, could be estimated from MR measurements of the myelin volume fraction and fiber/axon volume fraction (Stikov et al., 2015).

As discussed above and summarized in Fig. 2, there are many quantitative MRI parameters that provide complementary and overlapping information on the tissue microstructure. Combinations of these parametric maps are required to tease apart the different biological processes underlying structural plasticity and build a model of the time course of experience-induced changes. Once this model has been defined, it will become possible to devise an imaging protocol that most efficiently captures these changes.

Functional MRI

The behavioral improvements that characterize experience-induced plasticity are the result of local changes in brain function. While part of this functional adjustment arises from structural changes that scaffold local function, differences in neuronal encoding and neurovascular coupling may also contribute to alterations in functional response. Changes in neuronal activity have been the main focus of functional studies of learning-induced plasticity in humans, and a large number of studies have used the blood oxygen level dependent (BOLD) signal to characterize the functional learning process. In animals, learning and experience induce region- and task-specific long-term potentiation (LTP) and long-term depression (LTD) changes, or increases and decreases in neuronal activity. In humans, similar bidirectional changes have been observed. Paired associative stimulation (PAS) uses paired transcranial magnetic stimulation (TMS) pulses over the right and left motor cortex to manipulate the amplitude of the motor evoked potential (MEP)—a measure of cortical excitability. Studies of this phenomenon have shown that synchronized pulses lead to potentiation of the MEP in an LTP-like fashion, while asynchronous pulses lead to a

reduction of the MEP in an LTD-like fashion (Conde et al., 2013; Stefan et al., 2000). Furthermore, numerous human imaging studies of learning have shown both localized increases and decreases in BOLD signal (Albouy et al., 2012; Karni et al., 1995; King et al., 2013; Steele and Penhune, 2010). Interpretation of this signal is not straightforward, however, since the BOLD signal suffers from considerable physiological ambiguity (Buxton, 2010).

The relationship between functional and structural changes is highly complex. The changes observed using MRI in both modalities do not necessarily coincide spatially or temporally, as these may arise from partially independent processes, or changes at the network level. Few studies have characterized functional and structural changes within the same group of participants (Ilg et al., 2008; Schmidt-Wilcke et al., 2010; Taubert et al., 2011; Valkanova et al., 2014). Furthermore, plasticity is also influenced by a variety of factors including age and genetic and environmental influences on nerve growth factor levels and vascular integrity (Dinai et al., 2014; Licht et al., 2011; Valkanova et al., 2014). Functional changes may, therefore, only take their full meaning when combined with measures of behavior and the underlying structural, vascular, and metabolic environment.

Furthermore, characterization of purely local information may be misleading, since functional changes following training may also occur at the network level. Because invasive methods cannot easily probe network effects, little information exists in the animal literature about possible network-level plastic changes. Some of these questions can be addressed using MRI, and especially BOLD functional connectivity analysis.

Functional connectivity

Functional connectivity is an analysis technique used to identify networks of functionally coupled brain regions. In the context of plasticity, functional connectivity is predominantly estimated by means of resting-state or intrinsic connectivity, which uses the spontaneous fluctuations of the BOLD signal in the absence of a specific task (Biswal et al., 1995). As such, this technique requires only the acquisition of standard whole-brain BOLD data over 5–20 minutes depending on the study. Spontaneous BOLD signal fluctuations are thought to have a similar time course in well-connected brain areas and be the result of synchronized neuronal and cellular activity (Du et al., 2014). Identification of spatial components with similar BOLD time courses may therefore reflect networks of functionally connected areas. It is postulated that plasticity-induced network-level changes will result in increased resting functional connectivity between task-relevant areas.

Functional connectivity has been used to show brain plasticity induced by motor training (Lewis et al., 2009; Taubert et al., 2011; Young et al., 2014), exercise (Rajab et al., 2014; Voss et al., 2010), cognitive training (Mackey et al., 2013; Voss et al., 2012), and brain stimulation (Kuo et al., 2013; Polanía et al., 2012; Sehm et al., 2012), as well as sustained changes following a single session of a neurofeedback paradigm (Harmelech et al., 2013). Furthermore, recent results obtained using longitudinal learning paradigms indicate that changes in intrinsic functional connectivity may precede behavioral and structural changes (Kelly and Castellanos, 2014; Ma et al., 2011; Taubert et al., 2011). The growing interest in this type of analysis stems from its task independence (which makes it particularly suited to patient studies) and its ability to capture both local and global aspects of brain plasticity. However, intrinsic functional connectivity is also sensitive to many physiological factors like partial sleep deprivation (De Havas et al., 2012), stress (Soares et al., 2013), caffeine intake (Rack-Gomer et al., 2009), or chronotype (Blautzik et al., 2013).

Preprocessing of data to remove artifacts, spurious signal, and drifts is an important component of this technique, and careful elimination of noise is often essential. A variety of noise correction schemes have been proposed over the years (Birn, 2012; Birn et al., 2008; Biswal et al., 1995; Chang and Glover, 2009; Cordes et al., 2001; Weissenbacher et al., 2009), but new analysis techniques continue to be developed. Recent developments in motion correction algorithms can, for example, better account for micro movements in the sub-millimeter range (Power et al., 2014; Satterthwaite et al., 2013; Van Dijk et al., 2012). Also, a promising recent approach to remove noise exploits the different behavior of unwanted noise components and BOLD signal using a multi-echo sequence and independent component analysis (ICA) (Kundu et al., 2012, 2013). The automatic detection of non-neural ICA components in data from common sequences makes this technique accessible to a wider audience (Griffanti et al., 2014).

One limitation of fMRI data is its low temporal sampling rate compared with its high spatial dimensionality. This is problematic as there are not enough independent data points to estimate all possible functional connections. Sparse methods address this limitation by enforcing a reduced number of connections on this otherwise underdetermined system. Recently, sparse methods have been successfully applied to estimate intrinsic functional connectivity (Eavani et al., 2015; Ryali et al., 2012; Varoquaux and Craddock, 2013; Varoquaux et al., 2010). While the inherent assumption of a sparsely connected brain may be debatable, the methods perform empirically better (Smith et al., 2011). Another approach to increase temporal sampling involves new acceleration acquisition techniques such as multiband acquisitions to acquire several slices simultaneously (Liao et al., 2013) and more sophisticated k-space acquisition trajectories (Lee et al., 2013). However, the benefit of these fast acquisition techniques is limited as the majority of the power is contained in the low frequency range (Shmuel and Leopold, 2008).

While the aforementioned techniques improve functional connectivity estimation between brain areas, the careful selection of these regions remains crucial to reduce the number of statistical tests and to improve the signal-to-noise ratio of the functional signal. ROIs covering the whole cortex, based on recent advances in the construction of functional atlases (Craddock et al., 2012; Gordon et al., 2014; Power et al., 2011; Wig et al., 2013; Yeo et al., 2011), allow a whole-brain approach to brain plasticity. This whole-brain approach taps into one of the main strengths of MR and represents one of the few handles we have on brain-wide changes in network dynamics following experience-induced plasticity.

More work is needed to interpret functional connectivity changes in terms of plasticity beyond noting that some network change has occurred. Multi-modal acquisitions combining functional plasticity and other advanced functional imaging techniques will be needed to interpret these network changes in terms of neuronal, metabolic, and vascular changes. Furthermore, combination with more direct neuronal measures such as MEG and/or EEG may be useful to understand more specifically the neuronal component. For this type of work, functional connectivity analysis can most readily be used to define the regions where network changes are thought to occur. These network maps can then be used for ROI averaging of quantitative physiological and microstructure parameters. The network-level functional changes could also be used to predict the location of downstream structural changes (Taubert et al., 2011).

Vascular and metabolic imaging

Studies of neuroplasticity typically use the BOLD signal to assess brain function. However, the BOLD signal represents a relative change from an unknown baseline, and arises from an ambiguous mixture of blood flow, blood volume, and oxidative metabolism. This ambiguity results in a relatively low reproducibility (Krieger et al., 2014; Leontiev and Buxton, 2007) and reduces the inferences that can be made from a longitudinal change in signal. Therefore, while experience-driven BOLD signal decreases and increases indicate that some change has happened, it is impossible to know if this change is neuronal or vascular in nature (or both) with only a BOLD signal. This is particularly problematic given the indication that vascular changes such as angiogenesis may

be an important component of the experience-induced plasticity process (Kerr et al., 2010). Furthermore, animal studies indicate that not only is increased cerebral blood flow (CBF) important to support the increased activity associated with LTP, but it may be necessary for LTP to occur (Kerr et al., 2010).

More physiologically specific techniques may be used to measure vascular and metabolic properties that are necessary to refine the inferences drawn from neuroimaging research. Other MR techniques exist to study every BOLD signal subcomponent and, while they generally have a lower signal-to-noise ratio (SNR) than BOLD, they have been shown to provide greater physiological specificity and reproducibility (Krieger et al., 2014; Leontiev and Buxton, 2007). Furthermore, the BOLD signal observed could be anchored to changes in EEG and/or MEG signals, which would provide more direct evidence for neuronal changes.

Cerebral blood flow can be measured non-invasively using arterial spin labeling (ASL) (Detre et al., 1994). This technique uses an inversion pulse to label the blood before it arrives in the brain, then uses standard functional imaging readouts to capture the signal as the magnetic label exchanges with tissue water. A measure of tissue perfusion is obtained when this "labeled" image is subtracted from an identical image without label. This can be done during a task to obtain relative perfusion change or can be used in combination with a kinetic model to estimate absolute perfusion in ml/100 g tissue/min. Many labeling schemes have been developed, but pseudo-continuous ASL (pCASL) has been shown to be the most reliable (Chen et al., 2011). Despite its advantages in specificity and its ability to measure baseline information, ASL has only been used to assess experience-induced plasticity in a few studies so far (Burdette et al., 2010; Chapman et al., 2015; Fernandez-Seara et al., 2009; Mozolic et al., 2010). This may be due to the fact that, until recently, ASL sequences were not widely available. ASL also suffers from a fairly low SNR in populations with compromised vasculature and when measuring the low amplitude responses typically associated with the complex functional contrasts used to identify specific cognitive domains. Improvements in hardware and software have recently made this technique more accessible, and it may now be possible to use this technique to start addressing questions on the vascular contribution (both in terms of baseline or evoked blood flow changes and angiogenesis) to training-induced anatomical and functional changes. A typical pCASL sequence has a repetition time (TR) of around 4–5 seconds. For baseline blood flow, it has been shown that at least 40 tag-control pairs are needed for the signal to stabilize (Murphy et al., 2011), resulting in an acquisition time of about 5 minutes.

Cerebral blood volume can be measured using the vascular space occupancy (VASO) technique (Lu et al., 2003). This technique also uses magnetically labeled blood as an endogenous contrast agent, but in this case, all spins in the brain are inverted and the labeled image is acquired as the blood reaches its null point. Therefore, this image is acquired with no contribution from static blood water spins and is subtracted from an image where all spins contribute. This technique is sensitive to relative changes in total cerebral blood volume. While VASO is a promising technique for the study of neuroplasticity, due to its higher SNR as compared to ASL, to our knowledge, it has not yet been used in this context. VASO has been shown to have greater spatial specificity than BOLD and can be used at higher field strengths to study laminar functional activity (Huber et al., 2015). VASO is a dynamic technique and, depending on implementation, has a TR of 1.5–3 seconds. A related technique called inflow VASO (iVASO) has been developed to measure both relative changes in and resting arterial blood volume (Donahue et al., 2010; Hua et al., 2011). Venous blood volume (both evoked and at baseline) may also be measured using a biophysical model of the deoxyhemoglobin-induced changes in R2* during a hyperoxia manipulation (Blockley et al., 2012; Bulte et al., 2007). By allowing measurement of baseline CBV, these two techniques are particularly promising for the study of learning-induced angiogenesis. Both these techniques have not, however, been used extensively and may require additional expertise for their efficient implementation.

Oxidative metabolism can be estimated using a family of techniques called calibrated fMRI. These techniques typically use a combination of BOLD, ASL, and a breathing manipulation (such as hypercapnia, where the participant breathes air mixed with a low percentage of carbon dioxide) to estimate the purely vascular component of the BOLD response. This calibration procedure then allows the extraction of the relative change in oxidative metabolism from task-induced BOLD and ASL responses using a biophysical model (Chiarelli et al., 2007; Davis et al., 1998; Gauthier and Hoge, 2013). This technique has been shown to be more reproducible than BOLD (Krieger et al., 2014; Leontiev and Buxton, 2007), but has yet to be used to study experience-induced plasticity. These techniques have recently been extended to allow measurement of baseline oxidative metabolism (Bulte et al., 2012; Gauthier and Hoge, 2012; Wise et al., 2013), which could be highly relevant to the study of plasticity since it is likely that synaptogenesis, neurogenesis, gliogenesis, and glial hypertrophy are associated with increases in local baseline metabolism. These calibrated fMRI experiments require the use of a dual-echo ASL sequence to measure CBF and BOLD simultaneously and typical gas experiment durations are between 10–18 minutes.

Quantitative susceptibility mapping (QSM) can also be used to estimate local oxygen extraction fraction from cortical veins (Fan et al., 2014). This technique is based on the fact that the paramagnetic properties of deoxyhemoglobin create a susceptibility shift between veins and tissue. By quantifying this shift through QSM reconstruction (see section 2.1.3), we can directly measure the oxygenation fraction. While this technique provides good SNR in fairly large cortical veins, the quality of OEF estimates is highly dependent on partial volume effects and therefore resolution. These images can be acquired in around 5 minutes for a resolution of around 1.0 mm isotropic, but acquisition time for higher resolutions are longer (around 15 minutes for 0.6 mm isotropic). Therefore, while in isolation, this technique is unlikely to provide fine-enough resolution at 3 T to measure the localized changes associated with learning, it may be useful for the study of more global manipulations such as exercise training. Furthermore, combinations of the above-mentioned techniques would be particularly interesting for the study of neuroplasticity as they would help determine whether BOLD decreases during learning are due to increased baseline metabolism or a reduction in metabolic response amplitude.

Other techniques exist to study oxidative metabolism, including TRUST (T2-Relaxation-Under-Spin-Tagging), qBOLD (quantitative BOLD) (He and Yablonskiy, 2007), R2′ (1/T2′) methods (Blockley et al., 2012), and QUiXOTIC (QUantitative Imaging of eXtraction of oxygen and TIssue consumption). All these techniques are promising, but since calibrated fMRI and QSM also allow simultaneous measurement of various vascular parameters, they may be more useful for studying plasticity. A review of these different techniques, their advantages and disadvantages can be found in Christen and colleagues (Christen et al., 2013).

It is thought that plasticity is highly dependent on the local environment: the underlying dynamic range of neuronal, vascular, and metabolic resources (Huang et al., 2015; List et al., 2013; Murphy et al., 2014; Pearson-Fuhrhop and Cramer, 2010). In populations where the neuronal environment may be compromised (e.g. aging and disease), measurement of this environment may be valuable. Vascular integrity may be partly assessed, for example, through blood flow measurements and measurements of vascular reactivity (Gauthier et al., 2013; Goode et al., 2009). Vascular reactivity is typically assessed using the CBF or BOLD response to a purely vascular challenge such as carbon dioxide inhalation. Interestingly, both these sources of information about the neuronal environment are measured by default during a calibrated fMRI experiment. Therefore, by measuring oxidative metabolism, one may also obtain other important information for the characterization of the metabolic and vascular environment. Furthermore, while more

physiologically specific imaging techniques may help determine the nature of experience-induced functional changes, these techniques are typically used to assess localized changes. This localized information must, however, also be understood within a more global context since local brain areas do not typically work in isolation.

MRI of angiogenesis

Angiogenesis has been observed in rodents in response to environmental enrichment (Black et al., 1987; Sirevaag et al., 1988) and the Morris water maze paradigm (Kerr et al., 2010). In humans, evidence of angiogenesis has been observed almost exclusively in tumor growth, but it is possible that experience-induced plasticity also leads to changes in blood vessel density. For example, a study by Pereira et al. shows localized changes in contrast-enhanced measurement of baseline CBV following exercise training which may be indicative of angiogenesis (Pereira et al., 2007). While the resulting small-scale local changes in capillaries cannot be imaged directly with non-invasive techniques, increased microvascular density is expected to result in changes in local blood volume and possibly blood flow (Boehm-Sturm et al., 2013; Zechariah et al., 2013). This is an example whereby functional techniques can be used to indirectly investigate structural change.

The blood flow component, baseline perfusion, can be imaged using ASL. Blood volume measurements may involve the combination of several techniques. Complete resting absolute blood volume cannot be measured using current non-contrast-enhanced MRI techniques, but relative blood volume change can be measured using VASO, baseline arterial blood volume with iVASO, and baseline venous blood volume with a combination of BOLD measurements and end-tidal oxygen concentration sampling during hyperoxia. VASO during a task or hypercapnia manipulation could help uncover evidence of angiogenesis, as it is likely that additional capillaries result in a larger blood volume response to a vasodilatory stimulus. iVASO or hyperoxic fMRI could help uncover evidence for increased baseline CBV. While these techniques could yield results consistent with angiogenesis and should be tested within the context of plasticity studies, increased perfusion and CBV may not provide conclusive evidence for angiogenesis. Similar changes could arise from a variety of other causes, such as changes in neurovascular coupling (Fig. 2). Furthermore, the absence of an observed effect does not discount the presence of angiogenesis, given the relatively low SNR and sensitivity of these techniques and the large voxel sizes necessary at 3 T.

In the future, other techniques such as vessel size imaging could be used to address this question. Vessel size imaging uses the spin and gradient echo signal difference to a gas manipulation (typically hyperoxia) or to a bolus of contrast agent to estimate the average vessel size in a voxel (Germuska and Bulte, 2014; Jochimsen et al., 2010). Though this technique is currently not widely available, it could in the future be used to establish whether there is a shift toward smaller vessels during learning-induced plasticity, consistent with increased microvascular density following angiogenesis.

Harnessing specificity

We have described a broad range of advanced MRI techniques that can be used to probe the changes in structure, connectivity, and function of the entire brain over the course of learning. These techniques provide additional specificity compared to more common approaches. This specificity addresses two important limitations that were previously raised. Firstly, the quantitative nature of many of these techniques minimizes the impact of methodological confounds. This is particularly important in longitudinal learning-induced plasticity studies, as the effects to be detected are small. Furthermore, quantitative indices can be compared across studies, sites, and populations. These advantages will benefit the field of plasticity by facilitating the integration of different studies to build a mechanistic model of learning. Secondly, these MRI techniques can be used to better characterize the underlying cellular mechanisms that collectively give rise to macroscopic changes in tissue volume or function. Assuming that it is an accumulation of such changes that lead to the macroscopic effects detected by MRI, the greater specificity of these techniques could potentially make them more sensitive to subtle changes in the early time course of learning, or to subtle normalization effects that occur later.

Though advanced and quantitative MRI has many advantages, there is still a place for the conventional MRI techniques. Due to their high SNR and sensitivity, these conventional techniques may be best suited to detect the presence of a change. Advanced MRI techniques can be used in a complementary manner to investigate the multiple (physiological) sources of these changes. One way to harness the strengths of both approaches would be to use conventional MRI to delineate ROIs, and then measure the qMRI changes that occur within these ROIs. This has the advantage of reducing the dimensionality of the data and thus reducing the number of multiple comparisons. The latter is particularly advantageous for qMRI techniques that are less SNR efficient.

The greater specificity of the MR techniques presented here can take two forms. While some techniques are more biologically specific (such as ASL versus BOLD), some techniques may be more "biophysically specific," without providing additional information about the underlying biological properties. For example, T1 values represent a more faithful representation of tissue properties than T1-weighted values, allowing a more specific characterization of different tissues, their changes over time and comparison between groups. But it is not possible to ascribe specific biological interpretations to changes in T1 over time, since this biophysical property is known to arise from several biological features or cellular mechanisms.

Even given the gain in specificity of these techniques, there are no one-to-one mappings between these MR measures and individual plasticity mechanisms (see Figs. 1 and 2). The added-value of these techniques would be even greater if anchored to a model of plasticity. For instance, it is easier to interpret MR changes with knowledge of the timeline of the putative cellular mechanisms, and the relative composition of brain tissue. These mechanisms have been discussed in multiple studies (for e.g. Kleim et al., 2004; Sampaio-Baptista et al., 2014for a discussion), yet there is a paucity of unifying mechanistic models of the timeline of plasticity to explain the observed MR changes. Partial model elements have recently been proposed, however. For example, Johansen-Berg et al. propose a timeline of the cellular mechanisms that could cause a decrease in mean diffusivity in the hippocampus (Johansen-Berg et al., 2012).

In summary, there is no silver bullet. While the ultimate objective is to design a lean imaging protocol to study plasticity, we currently lack crucial knowledge about the MR signature of plasticity to achieve this. A single MR contrast cannot alone be used to describe or quantify plasticity due to the different time courses of the multiple biological mechanisms at play. Comprehensive multi-modal longitudinal MRI studies are necessary to build models of plasticity that are anchored in biological findings from animal models. Once a model has been defined, the focus can shift to developing simpler imaging protocols to efficiently capture specific features of the model.

Plasticity models would greatly benefit from more animal studies combining MRI and histology, such as Blumenfeld-Katzir et al. (2011), Hofstetter et al. (2013), Lerch et al. (2011), Sagi et al. (2012), and Sampaio-Baptista et al. (2013). Animal studies offer a unique opportunity to study longitudinal changes in brain structure using MRI as well as final high-resolution ex vivo MRI and histological measures while controlling for genetic and environmental factors (Lerch et al., 2012). Ex vivo animal imaging is a good opportunity to acquire images at higher resolutions, using quantitative techniques that are limited in SNR efficiency (such as quantitative MT and MWF), or to sample a wider range of MR contrasts to determine which are most sensitive or useful

for in vivo human imaging. Unfortunately, ex vivo imaging also has serious disadvantages since the entire micro-environment changes post-mortem, with temperature differences and fixation. Nevertheless, ex vivo and in vivo animal imaging can be used in the context of translational research to bridge findings from invasive animal studies and in vivo human neuroimaging.

The microstructural events that lead to macroscopic structural and functional changes in the brain will also depend on the local neural environment, i.e. the capacity for plasticity of different brain areas, which can vary due to age, genetics, environmental influences, neurovascular health, and disease. For example, the brain is plastic throughout the lifespan, but it is most plastic during a window of neurodevelopment, which may vary per structure. MRI can also be used to evaluate the local neural environment prior to learning. MRI has been used in this context to predict subsequent performance and plasticity from structure (Sampaio-Baptista et al., 2014), and to study the structural basis of inter-individual differences in human behavior and cognition (Kanai and Rees, 2011). Helbling et al. used quantitative MR myelin markers (relaxometry and MT measures) to predict functional responses detected using MEG, exemplifying the potential for structure-function relationship investigations at the microstructural level (Helbling et al., 2015). Quantitative MRI could provide a more accurate and reliable portrait of the local tissue environment.

Future promise of multi-modal MRI

The imaging techniques we reviewed are more biologically specific, which can help us interpret the complex changes occurring during plasticity. However, we cannot capture this complex process using a single imaging technique. Furthermore, from a technical standpoint, some image contrasts are less appropriate for investigating the cortex (e.g., due to limitations in resolution) or may be interpreted differently depending on the tissue compartment. Thus, we are not merely suggesting to acquire T1 maps instead of T1-weighted images and ASL instead of BOLD fMRI. Although this is a good first step, we are suggesting a much larger step toward multi-contrast MRI to get a comprehensive and refined picture of the longitudinal process of learning.

Although we may not be able to disentangle and quantify the contribution of different cellular mechanisms, different phases in the time course of learning will be characterized by distinct MR fingerprints: a unique inter-contrast relationship of longitudinal MR changes. In other words, by combining multiple MR contrasts that change over time, we can characterize and distinguish each time point. This fingerprint can also be used to measure how the neural environment can then affect performance. The objective is not to analyze and interpret the contrasts individually, but to integrate them. This can be performed as a simple co-visualization of different contrasts in space and/or time, or using more sophisticated approaches of data fusion or multi-variate statistics.

Multi-modal qMRI may seem ambitious at the moment, but technical advances already on the horizon will soon make this more accessible. Several technological advances have improved the sensitivity of MRI scanners, including higher magnetic field strengths and multi-channel coils. The advent of accelerated parallel imaging techniques has also led to greater imaging efficiency and resolution. Simultaneous multi-slice or multiband imaging, for instance, can now be used with functional imaging (Moeller et al., 2010) and diffusion-weighted imaging (Eichner et al., 2014; Setsompop et al., 2012) to dramatically increase image resolution and/or sampling rate. Stronger gradients systems allow us to increase the spatial resolution of images and to enhance diffusion-weighting to probe intracellular microstructure (McNab et al., 2013). These hardware improvements, combined with novel pulse sequences and post-processing techniques, will continue to enhance the quality, versatility, and efficiency of MRI. These technical developments will also allow us to acquire additional image contrasts within a single scanning session.

There are several advantages to higher resolution imaging. Firstly, image segmentation will be more precise, enhancing sensitivity to subtle shifts in tissue boundaries. The reduced partial volume effects will help differentiate displacement of tissue boundaries from changes in local tissue microstructure. Higher image resolution will also allow the study of smaller brain structures that may exhibit specific (micro-) structural changes in the context of plasticity, such as the hippocampal subfields, layers within the cerebral cortex, and lobules of the cerebellum. It will also help us interpret MRI results near structural boundaries, for instance in WM fibers neighboring the cortex. Some of the imaging techniques described above are currently limited in terms of resolution or coverage, but developments that enhance SNR efficiency promise to make them more practical for studies of plasticity where the expected changes are local and subtle.

Conclusion

In this review, we describe a collection of advanced MRI techniques that have the potential to further our understanding of the morphological, microstructural, physiological, and connectivity changes that occur in the brain during the course of learning. The versatility of MRI allows several contrasts to be measured within a single session, allowing researchers to construct a multi-contrast fingerprint, a more nuanced expression of plasticity. This fingerprint could include conventional MRI contrasts in addition to the methods described herein, taking advantage of their higher sensitivity to guide our initial search for the location of changes. A unifying model of the timeline of potential biological mechanisms could enhance the interpretational power of the individual MR contrasts and their combined fingerprint.

Learning-induced plasticity is a complex, dynamic, whole-brain process; multi-modal MRI is a powerful tool to gain a comprehensive understanding of it. Future studies could use this tool to investigate these fundamental questions: how do we learn, why do some individuals learn faster than others, and how can we enhance our learning?

Acknowledgments

C.J.G. was funded by the Postdoctoral fellowships of the Fonds de recherche en santé du Québec and the Alexander von Humboldt Foundation. The authors would like to thank Dr. Nikolaus Weiskopf for helpful comments on the manuscript.

Appendix A. MRI Glossary

AD	Axial diffusivity
ASL	Arterial spin labeling
BOLD	Blood oxygen level dependent
B0	Static main magnetic field
$B1^{+/-}$	Radio frequency magnetic field. $B1^{+}$ refers to the pulsed transmission field and $B1^{-}$ refers to the receive field.
DBM	Deformation-based morphometry
DKI	Diffusion kurtosis imaging
DTI	Diffusion tensor imaging
DWI	Diffusion weighted imaging
FA	Fractional anisotropy
FLASH	Fast low angle shot, a.k.a. FFE (fast field echo), SPGR (spoiled gradient echo)
iVASO	inflow VASO
MD	Mean diffusivity
MP2RAGE	Magnetization prepared 2 rapid acquisition by gradient echo
MT(R)	Magnetization transfer (ratio)
MTV	Macromolecular tissue volume
MWF	Myelin water fraction
pCASL	Pseudo-continuous ASL
PD	Proton density

qBOLD	Quantitative BOLD
qMRI	Quantitative MRI
QSM	Quantitative susceptibility mapping
QUiXOTIC	Quantitative imaging of extraction of oxygen and tissue consumption
RD	Radial diffusivity
T	Tesla
TRUST	T2-relaxation-under-spin-tagging
T1	Longitudinal or spin-lattice relaxation time
T2*	T2* transverse relaxation time
T2	Transverse relaxation due to spin-spin interactions
T2'	Transverse relaxation due to magnetic field perturbations
VASO	Vascular space occupancy
VBM	Voxel-based morphometry
VFA	Variable flip angle

References

Abbas, Z., Gras, V., Möllenhoff, K., Oros-Peusquens, A.-M., Shah, N.J., 2015. Quantitative water content mapping at clinically relevant field strengths: a comparative study at 1.5 T and 3 T. Neuroimage 106, 404–413.

Akbik, F., Cafferty, W.B.J., Strittmatter, S.M., 2012. Myelin associated inhibitors: a link between injury-induced and experience-dependent plasticity. Exp. Neurol. 235, 43–52.

Albouy, G., Sterpenich, V., Vandewalle, G., Darsaud, A., Gais, S., Rauchs, G., Desseilles, M., Boly, M., Dang-Vu, T., Balteau, E., Degueldre, C., Phillips, C., Luxen, A., Maquet, P., 2012. Neural correlates of performance variability during motor sequence acquisition. Neuroimage 60, 324–331.

Alexander, D.C., Hubbard, P.L., Hall, M.G., Moore, E.A., Ptito, M., Parker, G.J.M., Dyrby, T.B., 2010. Orientationally invariant indices of axon diameter and density from diffusion MRI. Neuroimage 52, 1374–1389.

Alonso-Ortiz, E., Levesque, I.R., Pike, G.B., 2015. MRI-based myelin water imaging: a technical review. Magn. Reson. Med. 73, 70–81.

Ashburner, J., Friston, K.J., 2000. Voxel-based morphometry—the methods. Neuroimage 11, 805–821.

Assaf, Y., Basser, P.J., 2005. Composite hindered and restricted model of diffusion (CHARMED) MR imaging of the human brain. Neuroimage 27, 48–58.

Assaf, Y., Blumenfeld-Katzir, T., Yovel, Y., Basser, P.J., 2008. AxCaliber: a method for measuring axon diameter distribution from diffusion MRI. Magn. Reson. Med. 59, 1347–1354.

Baloch, S., Davatzikos, C., 2009. Morphological appearance manifolds in computational anatomy: groupwise registration and morphological analysis. Neuroimage 45, S73–85.

Barral, J.K., Gudmundson, E., Stikov, N., Etezadi-Amoli, M., Stoica, P., Nishimura, D.G., 2010. A robust methodology for in vivo T1 mapping. Magn. Reson. Med. 64, 1057–1067.

Basser, P.J., 1995. Inferring microstructural features and the physiological state of tissues from diffusion-weighted images. NMR Biomed. 8, 333–344.

Bazin, P.-L., Ye, C., Bogovic, J.A., Shiee, N., Reich, D.S., Prince, J.L., Pham, D.L., 2011. Direct segmentation of the major white matter tracts in diffusion tensor images. Neuroimage 58, 458–468.

Bazin, P.-L., Weiss, M., Dinse, J., Schäfer, A., Trampel, R., Turner, R., 2014. A computational framework for ultra-high resolution cortical segmentation at 7 Tesla. Neuroimage 93, 201–209.

Beaulieu, C., 2002. The basis of anisotropic water diffusion in the nervous system—a technical review. NMR Biomed. 15, 435–455.

Bengtsson, S.L., Nagy, Z., Skare, S., Forsman, L., Forssberg, H., Ullén, F., 2005. Extensive piano practicing has regionally specific effects on white matter development. Nat. Neurosci. 8, 1148–1150.

Birn, R.M., 2012. The role of physiological noise in resting-state functional connectivity. Neuroimage 62, 864–870.

Birn, R.M., Murphy, K., Bandettini, P.A., 2008. The effect of respiration variations on independent component analysis results of resting state functional connectivity. Hum. Brain Mapp. 29, 740–750.

Biswal, B., Yetkin, F.Z., Haughton, V.M., Hyde, J.S., 1995. Functional connectivity in the motor cortex of resting human brain using echo-planar MRI. Magn. Reson. Med. 34, 537–541.

Black, J.E., Sirevaag, A.M., Greenough, W.T., 1987. Complex experience promotes capillary formation in young rat visual cortex. Neurosci. Lett. 83, 351–355.

Black, J.E., Zelazny, A.M., Greenough, W.T., 1991. Capillary and mitochondrial support of neural plasticity in adult rat visual cortex. Exp. Neurol. 111, 204–209.

Blautzik, J., Vetter, C., Peres, I., Gutyrchik, E., Keeser, D., Berman, A., Kirsch, V., Mueller, S., Pöppel, E., Reiser, M., 2013. Classifying fMRI-derived resting-state connectivity patterns according to their daily rhythmicity. Neuroimage 71, 298–306.

Blockley, N.P., Griffeth, V.E., Buxton, R.B., 2012. A general analysis of calibrated BOLD methodology for measuring $CMRO_2$ responses: comparison of a new approach with existing methods. Neuroimage 60, 279–289.

Blumenfeld-Katzir, T., Pasternak, O., Dagan, M., Assaf, Y., 2011. Diffusion MRI of structural brain plasticity induced by a learning and memory task. PLoS One 6, e20678.

Boehm-Sturm, P., Farr, T.D., Adamczak, J., Jikeli, J.F., Mengler, L., Wiedermann, D., Kallur, T., Kiselev, V., Hoehn, M., 2013. Vascular changes after stroke in the rat: a longitudinal study using optimized magnetic resonance imaging. Contrast Media Mol. Imaging 8, 383–392.

Bogovic, J.A., Bazin, P.-L., Ying, S.H., Prince, J.L., 2013. Automated Segmentation of the Cerebellar Lobules Using Boundary Specific Classification and Evolution. Lecture Notes in Computer Science 7917 pp. 62–73.

Bookstein, F.L., 2001. "Voxel-based morphometry" should not be used with imperfectly registered images. Neuroimage 14, 1454–1462.

Bulte, D., Chiarelli, P., Wise, R., Jezzard, P., 2007. Measurement of cerebral blood volume in humans using hyperoxic MRI contrast. J. Magn. Reson. Imaging 26, 894–899.

Bulte, D.P., Kelly, M., Germuska, M., Xie, J., Chappell, M.A., Okell, T.W., Bright, M.G., Jezzard, P., 2012. Quantitative measurement of cerebral physiology using respiratory-calibrated MRI. Neuroimage 60, 582–591.

Burdette, J.H., Laurienti, P.J., Espeland, M.A., Morgan, A., Telesford, Q., Vechlekar, C.D., Hayasaka, S., Jennings, J.M., Katula, J.A., Kraft, R.A., Rejeski, W.J., 2010. Using network science to evaluate exercise-associated brain changes in older adults. Front. Aging Neurosci. 2, 23.

Buxton, R.B., 2010. Interpreting oxygenation-based neuroimaging signals: the importance and the challenge of understanding brain oxygen metabolism. Front. Neuroenerg. 2, 8.

Cahill, L.S., Steadman, P.E., Jones, C.E., Laliberté, C.L., Dazai, J., Lerch, J.P., Stefanovic, B., Sled, J.G., 2015. MRI-detectable changes in mouse brain structure induced by voluntary exercise. Neuroimage 113, 175–183.

Calamante, F., Tournier, J.D., Heidemann, R.M., Anwander, A., Jackson, G.D., Connelly, A., 2011. Track density imaging (TDI): validation of super resolution property. Neuroimage 56, 1259–1266.

Callaghan, M.F., Helms, G., Lutti, A., Mohammadi, S., Weiskopf, N., 2015. A general linear relaxometry model of R 1 using imaging data. Magn. Reson. Med. 73, 1309–1314.

Cercignani, M., 2010. Strategies for patient-control comparison of diffusion MR data. In: Jones, D.K. (Ed.), Diffusion MRI: Theory, Methods and Applications. Oxford University Press.

Chang, C., Glover, G.H., 2009. Effects of model-based physiological noise correction on default mode network anti-correlations and correlations. Neuroimage 47, 1448–1459.

Chapman, S.B., Aslan, S., Spence, J.S., Hart, J.J., Bartz, E.K., Didehbani, N., Keebler, M.W., Gardner, C.M., Strain, J.F., Defina, L.F., Lu, H., 2015. Neural mechanisms of brain plasticity with complex cognitive training in healthy seniors. Cereb. Cortex 25, 396–405.

Chavhan, G.B., Babyn, P.S., Jankharia, B.G., Cheng, H.L., Shroff, M.M., 2008. Steady-state MR imaging sequences: physics, classification, and clinical applications. Radiographics 28, 1147–1160.

Chen, Y., Wang, D.J.J., Detre, J.A., 2011. Test-retest reliability of arterial spin labeling with common labeling strategies. J. Magn. Reson. Imaging 33, 940–949.

Chiarelli, P.A., Bulte, D.P., Wise, R., Gallichan, D., Jezzard, P., 2007. A calibration method for quantitative BOLD fMRI based on hyperoxia. Neuroimage 37, 808–820.

Christen, T., Bolar, D.S., Zaharchuk, G., 2013. Imaging brain oxygenation with MRI using blood oxygenation approaches: methods, validation, and clinical applications. AJNR Am. J. Neuroradiol. 34, 1113–1123.

Cohen-Adad, J., Polimeni, J.R., Helmer, K.G., Benner, T., McNab, J.A., Wald, L.L., Rosen, B.R., Mainero, C., 2012. T2* mapping and B0 orientation-dependence at 7 T reveal cyto- and myeloarchitecture organization of the human cortex. Neuroimage 60, 1006–1014.

Concha, L., 2014. A macroscopic view of microstructure: using diffusion-weighted images to infer damage, repair, and plasticity of white matter. Neuroscience 276, 14–28.

Conde, V., Vollmann, H., Taubert, M., Sehm, B., Cohen, L.G., Villringer, A., Ragert, P., 2013. Reversed timing-dependent associative plasticity in the human brain through interhemispheric interactions. J. Neurophysiol. 109, 2260–2271.

Cordes, D., Haughton, V.M., Arfanakis, K., Carew, J.D., Turski, P.A., Moritz, C.H., Quigley, M.A., Meyerand, M.E., 2001. Frequencies contributing to functional connectivity in the cerebral cortex in "resting-state" data. Am. J. Neuroradiol. 22, 1326–1333.

Corouge, I., Fletcher, P.T., Joshi, S., Gouttard, S., Gerig, G., 2006. Fiber tract-oriented statistics for quantitative diffusion tensor MRI analysis. Med. Image Anal. 10, 786–798.

Craddock, R.C., James, G.A., Holtzheimer, P.E., Hu, X.P., Mayberg, H.S., 2012. A whole brain fMRI atlas generated via spatially constrained spectral clustering. Hum. Brain Mapp. 33, 1914–1928.

Czopka, T., ffrench-Constant, C., Lyons, D., 2013. Individual oligodendrocytes have only a few hours in which to generate new myelin sheaths invivo. Dev. Cell 25, 599–609.

Das, S.R., Avants, B.B., Pluta, J., Wang, H., Suh, J.W., Weiner, M.W., Mueller, S.G., Yushkevich, P.A., 2012. Measuring longitudinal change in the hippocampal formation from in vivo high-resolution T2-weighted MRI. Neuroimage 60, 1266–1279.

Davatzikos, C., 2004. Why voxel-based morphometric analysis should be used with great caution when characterizing group differences. Neuroimage 23, 17–20.

Davatzikos, C., Shen, D., Mohamed, A., Kyriacou, S.K., 2001. A framework for predictive modeling of anatomical deformations. IEEE Trans. Med. Imaging 20, 836–843.

Davis, T.L., Kwong, K.K., Weisskoff, R.M., Rosen, B.R., 1998. Calibrated functional MRI: mapping the dynamics of oxidative metabolism. Proc. Natl. Acad. Sci. U. S. A. 95, 1834–1839.

Dayan, E., Cohen, L.G., 2011. Neuroplasticity subserving motor skill learning. Neuron 72, 443–454.

De Havas, J.A., Parimal, S., Soon, C.S., Chee, M.W.L., 2012. Sleep deprivation reduces default mode network connectivity and anti-correlation during rest and task performance. Neuroimage 59, 1745–1751.

Deistung, A., Schäfer, A., Schweser, F., Biedermann, U., Güllmar, D., Trampel, R., Turner, R., Reichenbach, J.R., 2013a. High-resolution MR imaging of the human brainstem in vivo at 7 Tesla. Front. Hum. Neurosci. 7, 710.

Deistung, A., Schäfer, A., Schweser, F., Biedermann, U., Turner, R., Reichenbach, J.R., 2013b. Toward in vivo histology: a comparison of quantitative susceptibility mapping (QSM) with magnitude-, phase-, and R2*-imaging at ultra-high magnetic field strength. Neuroimage 65, 299–314.

Dell'Acqua, F., Simmons, A., Williams, S.C.R., Catani, M., 2013. Can spherical deconvolution provide more information than fiber orientations? Hindrance modulated orientational anisotropy, a true-tract specific index to characterize white matter diffusion. Hum. Brain Mapp. 34, 2464–2483.
Deoni, S.C., Peters, T.M., Rutt, B.K., 2005. High-resolution T1 and T2 mapping of the brain in a clinically acceptable time with DESPOT1 and DESPOT2. Magn. Reson. Med. 53, 237–241.
Detre, J.A., Zhang, W., Roberts, D.A., Silva, A.C., Williams, D.S., Grandis, D.J., Koretsky, A.P., Leigh, J.S., 1994. Tissue specific perfusion imaging using arterial spin labeling. NMR Biomed. 7, 75–82.
Dick, F., Tierney, A.T., Lutti, A., Josephs, O., Sereno, M.I., Weiskopf, N., 2012. In vivo functional and myeloarchitectonic mapping of human primary auditory areas. J. Neurosci. 32, 16095–16105.
Diedrichsen, J., Balsters, J.H., Flavell, J., Cussans, E., Ramnani, N., 2009. A probabilistic MR atlas of the human cerebellum. Neuroimage 46, 39–46.
Dill, V., Franco, A.R., Pinho, M.S., 2015. Automated methods for hippocampus segmentation: the evolution and a review of the state of the art. Neuroinformatics 13, 133–150.
Dinai, Y., Wolf, L., Assaf, Y., 2014. Combined neuroimaging and gene expression analysis of the genetic basis of brain plasticity indicates across species homology. Hum. Brain Mapp. 35, 5888–5902.
Ding, A.Y., Li, Q., Zhou, I.Y., Ma, S.J., Tong, G., McAlonan, G.M., Wu, E.X., 2013. MR diffusion tensor imaging detects rapid microstructural changes in amygdala and hippocampus following fear conditioning in mice. PLoS One 8.
Donahue, M.J., Sideso, E., MacIntosh, B.J., Kennedy, J., Handa, A., Jezzard, P., 2010. Absolute arterial cerebral blood volume quantification using inflow vascular-space-occupancy with dynamic subtraction magnetic resonance imaging. J. Cereb. Blood Flow Metab. 30, 1329–1342.
Dong, W.K., Greenough, W.T., 2004. Plasticity of nonneuronal brain tissue: roles in developmental disorders. Ment. Retard. Dev. Disabil. Res. Rev. 10, 85–90.
Dortch, R.D., Moore, J., Li, K., Jankiewicz, M., Gochberg, D.F., Hirtle, J.A., Gore, J.C., Smith, S.A., 2013. Quantitative magnetization transfer imaging of human brain at 7 T. Neuroimage 64, 640–649.
Draganski, B., May, A., 2008. Training-induced structural changes in the adult human brain. Behav. Brain Res. 192, 137–142.
Draganski, B., Gaser, C., Busch, V., Schuierer, G., Bogdahn, U., May, A., 2004. Neuroplasticity: changes in grey matter induced by training. Nature 427, 311–312.
Draganski, B., Kherif, F., Lutti, A., 2014. Computational anatomy for studying use-dependant brain plasticity. Front. Hum. Neurosci. 8, 380.
Du, C., Volkow, N.D., Koretsky, A.P., Pan, Y., 2014. Low-frequency calcium oscillations accompany deoxyhemoglobin oscillations in rat somatosensory cortex. Proc. Natl. Acad. Sci. U. S. A. 111, E4677–E4686.
Duyn, J.H., van Gelderen, P., Li, T.-Q., de Zwart, J.A., Koretsky, A.P., Fukunaga, M., 2007. High-field MRI of brain cortical substructure based on signal phase. Proc. Natl. Acad. Sci. U. S. A. 104, 11796–11801.
Eavani, H., Satterthwaite, T.D., Filipovych, R., Gur, R.E., Gur, R.C., Davatzikos, C., 2015. Identifying sparse connectivity patterns in the brain using resting-state fMRI. Neuroimage 105, 286–299.
Eichner, C., Setsompop, K., Koopmans, P.J., Lützkendorf, R., Norris, D.G., Turner, R., Wald, L.L., Heidemann, R.M., 2014. Slice accelerated diffusion-weighted imaging at ultra-high field strength. Magn. Reson. Med. 71, 1518–1525.
Erickson, K.I., Weinstein, A.M., Lopez, O.L., 2012. Physical activity, brain plasticity, and Alzheimer's disease. Arch. Med. Res. 43, 615–621.
Fan, A.P., Bilgic, B., Gagnon, L., Witzel, T., Bhat, H., Rosen, B.R., Adalsteinsson, E., 2014. Quantitative oxygenation venography from MRI phase. Magn. Reson. Med. 72, 149–159.
Fernandez-Seara, M.A., Aznarez-Sanado, M., Mengual, E., Loayza, F.R., Pastor, M.A., 2009. Continuous performance of a novel motor sequence leads to highly correlated striatal and hippocampal perfusion increases. Neuroimage 47, 1797–1808.
Fields, R.D., 2008. White matter in learning, cognition and psychiatric disorders. Trends Neurosci. 31, 361–370.
Fields, R.D., 2010. Change in the brain's white matter: The role of the brain's white matter in active learning and memory may be underestimated. Science 330, 768–769.
Fields, R.D., Araque, A., Johansen-Berg, H., Lim, S.-S., Lynch, G., Nave, K.-A., Nedergaard, M., Perez, R., Sejnowski, T., Wake, H., 2014. Glial biology in learning and cognition. Neuroscientist 20, 426–431.
Fischl, B., Wald, L.L., 2007. Phase maps reveal cortical architecture. Proc. Natl. Acad. Sci. U. S. A. 104, 11513–11514.
Fram, E.K., Herfkens, R.J., Johnson, G.A., Glover, G.H., Karis, J.P., Shimakawa, A., Perkins, T.G., Pelc, N.J., 1987. Rapid calculation of T1 using variable flip angle gradient refocused imaging. Magn. Reson. Imaging 5, 201–208.
Frost, M.A., Goebel, R., 2013. Functionally informed cortex based alignment: an integrated approach for whole-cortex macro-anatomical and ROI-based functional alignment. Neuroimage 83, 1002–1010.
Fujimoto, K., Polimeni, J.R., van der Kouwe, A.J.W., Reuter, M., Kober, T., Benner, T., Fischl, B., Wald, L.L., 2014. Quantitative comparison of cortical surface reconstructions from MP2RAGE and multi-echo MPRAGE data at 3 and 7 T. Neuroimage 90, 60–73.
Fukunaga, M., Li, T.Q., van Gelderen, P., de Zwart, J.A., Shmueli, K., Yao, B., Lee, J., Maric, D., Aronova, M.A., Zhang, G., Leapman, R.D., Schenck, J.F., Merkle, H., Duyn, J.H., 2010. Layer-specific variation of iron content in cerebral cortex as a source of MRI contrast. Proc. Natl. Acad. Sci. U. S. A. 107, 3834–3839.
Ganzetti, M., Wenderoth, N., Mantini, D., 2014. Whole brain myelin mapping using T1- and T2-weighted MR imaging data. Front. Hum. Neurosci. 8, 671.
Gautam, P., Anstey, K.J., Wen, W., Sachdev, P.S., Cherbuin, N., 2015. Cortical gyrification and its relationships with cortical volume, cortical thickness, and cognitive performance in healthy midlife adults. Behav. Brain Res. 287, 331–339.
Gauthier, C.J., Hoge, R.D., 2012. Magnetic resonance imaging of resting OEF and CMRO2 using a generalized calibration model for hypercapnia and hyperoxia. Neuroimage 60, 1212–1225.
Gauthier, C.J., Hoge, R.D., 2013. A generalized procedure for calibrated MRI incorporating hyperoxia and hypercapnia. Hum. Brain Mapp. 34, 1053–1069.
Gauthier, C.J., Madjar, C., Desjardins-Crépeau, L., Bellec, P., Bherer, L., Hoge, R.D., 2013. Age dependence of hemodynamic response characteristics in human functional magnetic resonance imaging. Neurobiol. Aging 34, 1469–1485.
Gerardin, E., Chételat, G., Chupin, M., Cuingnet, R., Desgranges, B., Kim, H.S., Niethammer, M., Dubois, B., Lehéricy, S., Garnero, L., Eustache, F., Colliot, O., 2009. Multidimensional classification of hippocampal shape features discriminates Alzheimer's disease and mild cognitive impairment from normal aging. Neuroimage 47, 1476–1486.
Germuska, M., Bulte, D.P., 2014. MRI measurement of oxygen extraction fraction, mean vessel size and cerebral blood volume using serial hyperoxia and hypercapnia. Neuroimage 92, 132–142.
Gibson, E.M., Purger, D., Mount, C.W., Goldstein, A.K., Lin, G.L., Wood, L.S., Inema, I., Miller, S.E., Bieri, G., Zuchero, J.B., Barres, B.A., Woo, P.J., Vogel, H., Monje, M., 2014. Neuronal activity promotes oligodendrogenesis and adaptive myelination in the mammalian brain. Science 344, 1252304.
Girard, G., Whittingstall, K., Deriche, R., Descoteaux, M., 2014. Towards quantitative connectivity analysis: reducing tractography biases. Neuroimage 98, 266–278.
Glasser, M.F., Van Essen, D.C., 2011. Mapping human cortical areas in vivo based on myelin content as revealed by T1- and T2-weighted MRI. J. Neurosci. 31, 11597–11616.
Glenn, G.R., Helpern, J.A., Tabesh, A., Jensen, J.H., 2015. Quantitative assessment of diffusional kurtosis anisotropy. NMR Biomed. 28, 448–459.
Goode, S.D., Krishan, S., Alexakis, C., Mahajan, R., Auer, D.P., 2009. Precision of cerebrovascular reactivity assessment with use of different quantification methods for hypercapnia functional MR imaging. AJNR Am. J. Neuroradiol. 30, 972–977.
Gordon, E.M., Laumann, T.O., Adeyemo, B., Huckins, J.F., Kelley, W.M., Petersen, S.E., 2014. Generation and evaluation of a cortical area parcellation from resting-state correlations. Cereb. Cortex bhu239.
Gould, E., Beylin, A., Tanapat, P., Reeves, A., Shors, T.J., 1999. Learning enhances adult neurogenesis in the hippocampal formation. Nat. Neurosci. 2, 260–265.
Griffanti, L., Salimi-Khorshidi, G., Beckmann, C.F., Auerbach, E.J., Douaud, G., Sexton, C.E., Zsoldos, E., Ebmeier, K.P., Filippini, N., Mackay, C.E., Moeller, S., Xu, J., Yacoub, E., Baselli, G., Ugurbil, K., Miller, K.L., Smith, S.M., 2014. ICA-based artefact removal and accelerated fMRI acquisition for improved resting state network imaging. Neuroimage 95, 232–247.
Grydeland, H., Walhovd, K.B., Tamnes, C.K., Westlye, L.T., Fjell, A.M., 2013. Intracortical myelin links with performance variability across the human lifespan: results from T1- and T2-weighted MRI myelin mapping and diffusion tensor imaging. J. Neurosci. 33, 18618–18630.
Grydeland, H., Westlye, L.T., Walhovd, K.B., Fjell, A.M., 2015. Intracortical posterior cingulate myelin content relates to error processing: results from T1- and T2-weighted MRI myelin mapping and electrophysiology in healthy adults. Cereb. Cortex.
Gryga, M., Taubert, M., Dukart, J., Vollmann, H., Conde, V., Sehm, B., Villringer, A., Ragert, P., 2012. Bidirectional gray matter changes after complex motor skill learning. Front. Syst. Neurosci. 6, 37.
Haacke, E.M., Xu, Y., Cheng, Y.-C.N., Reichenbach, J.R., 2004. Susceptibility weighted imaging (SWI). Magn. Reson. Med. 52, 612–618.
Haddock, B., Larsson, H.B.W., Hansen, A.E., Rostrup, E., 2013. Measurement of brain oxygenation changes using dynamic T1-weighted imaging. Neuroimage 78, 7–15.
Harkins, K.D., Xu, J., Dula, A.N., Li, K., Valentine, W.M., Gochberg, D.F., Gore, J.C., Does, M.D., 2015. The microstructural correlates of t 1 in white matter. Magn. Reson. Med.
Harmelech, T., Preminger, S., Wertman, E., Malach, R., 2013. The day-after effect: long term, Hebbian-like restructuring of resting-state fMRI patterns induced by a single epoch of cortical activation. J. Neurosci. 33, 9488–9497.
Haroutunian, V., Katsel, P., Roussos, P., Davis, K.L., Altshuler, L.L., Bartzokis, G., 2014. Myelination, oligodendrocytes, and serious mental illness. Glia 62, 1856–1877.
He, X., Yablonskiy, D.A., 2007. Quantitative BOLD: mapping of human cerebral deoxygenated blood volume and oxygen extraction fraction: default state. Magn. Reson. Med. 57, 115–126.
Hebb, D.O., 1949. The Organization of Behavior. Wiley & Sons, New York.
Heidemann, R.M., Anwander, A., Feiweier, T., Knösche, T.R., Turner, R., 2012. k-space and q-space: Combining ultra-high spatial and angular resolution in diffusion imaging using ZOOPPA at 7T. Neuroimage 60, 967–978.
Helbling, S., Teki, S., Callaghan, M.F., Sedley, W., Mohammadi, S., Griffiths, T.D., Weiskopf, N., Barnes, G.R., 2015. Structure predicts function: combining non-invasive electrophysiology with in-vivo histology. Neuroimage 108, 377–385.
Helms, G., Dathe, H., Kallenberg, K., Dechent, P., 2008. High-resolution maps of magnetization transfer with inherent correction for RF inhomogeneity and T1 relaxation obtained from 3D FLASH MRI. Magn. Reson. Med. 60, 1396–1407.
Helms, G., Draganski, B., Frackowiak, R., Ashburner, J., Weiskopf, N., 2009. Improved segmentation of deep brain grey matter structures using magnetization transfer (MT) parameter maps. Neuroimage 47, 194–198.
Helms, G., Dathe, H., Dechent, P., 2010. Modeling the influence of TR and excitation flip angle on the Magnetization Transfer Ratio (MTR) in human brain obtained from 3D spoiled gradient echo MRI. Magn. Reson. Med. 64, 177–185.
Henkelman, R.M., Stanisz, G.J., Graham, S.J., 2001. Magnetization transfer in MRI: a review. Nucl. Magn. Reson. Biomed. 14, 57–64.
Hofstetter, S., Tavor, I., Tzur Moryosef, S., Assaf, Y., 2013. Short-term learning induces white matter plasticity in the fornix. J. Neurosci. 33, 12844–12850.
Holtmaat, A., Svoboda, K., 2009. Experience-dependent structural synaptic plasticity in the mammalian brain. Nat. Rev. Neurosci. 10, 647–658.

Horowitz, A., Barazany, D., Tavor, I., Bernstein, M., Yovel, G., Assaf, Y., 2015. In vivo correlation between axon diameter and conduction velocity in the human brain. Brain Struct. Funct. 220, 1777–1788.
Hua, J., Qin, Q., Donahue, M.J., Zhou, J., Pekar, J.J., van Zijl, P.C., 2011. Inflow-based vascular-space-occupancy (iVASO) MRI. Magn. Reson. Med. 66, 40–56.
Huang, T.-T., Leu, D., Zou, Y., 2015. Oxidative stress and redox regulation on hippocampal-dependent cognitive functions. Arch. Biochem. Biophys. 576, 2–7.
Huber, L., Goense, J., Kennerley, A.J., Trampel, R., Guidi, M., Reimer, E., Ivanov, D., Neef, N., Gauthier, C.J., Turner, R., Möller, H.E., 2015. Cortical lamina-dependent blood volume changes in human brain at 7 T. Neuroimage 107, 23–33.
Hutton, C., Draganski, B., Ashburner, J., Weiskopf, N., 2009. A comparison between voxel-based cortical thickness and voxel-based morphometry in normal aging. Neuroimage 48, 371–380.
Hyde, K.L., Lerch, J., Norton, A., Forgeard, M., Winner, E., Evans, A.C., Schlaug, G., 2009. Musical training shapes structural brain development. J. Neurosci. 29, 3019–3025.
Ilg, R., Wohlschlager, A.M., Gaser, C., Liebau, Y., Dauner, R., Woller, A., Zimmer, C., Zihl, J., Muhlau, M., 2008. Gray matter increase induced by practice correlates with task-specific activation: a combined functional and morphometric magnetic resonance imaging study. J. Neurosci. 28, 4210–4215.
Innocenti, G.M., Caminiti, R., Aboitiz, F., 2015. Comments on the paper by Horowitz et al. (2014). pp. 3–4.
Jensen, J.H., Helpern, J.A., Ramani, A., Lu, H., Kaczynski, K., 2005. Diffusional kurtosis imaging: the quantification of non-Gaussian water diffusion by means of magnetic resonance imaging. Magn. Reson. Med. 53, 1432–1440.
Jiang, X., Li, H., Xie, J., Zhao, P., Gore, J.C., Xu, J., 2015. Quantification of cell size using temporal diffusion spectroscopy. Magn. Reson. Med.
Jochimsen, T.H., Ivanov, D., Ott, D.V., Heinke, W., Turner, R., Moller, H.E., Reichenbach, J.R., 2010. Whole-brain mapping of venous vessel size in humans using the hypercapnia-induced BOLD effect. Neuroimage 51, 765–774.
Johansen-Berg, H., 2010. Behavioural relevance of variation in white matter microstructure. Curr. Opin. Neurol. 23, 351–358.
Johansen-Berg, H., Della-Maggiore, V., Behrens, T.E.J., Smith, S.M., Paus, T., 2007. Integrity of white matter in the corpus callosum correlates with bimanual co-ordination skills. Neuroimage 36.
Johansen-Berg, H., Baptista, C.S., Thomas, A.G., 2012. Human structural plasticity at record speed. Neuron 73, 1058–1060.
Jones, D.K., Cercignani, M., 2010. Twenty-five pitfalls in the analysis of diffusion MRI data. NMR Biomed. 23, 803–820.
Jones, D.K., Knösche, T.R., Turner, R., 2013. White matter integrity, fiber count, and other fallacies: the do's and don'ts of diffusion MRI. Neuroimage 73, 239–254.
Kanai, R., Rees, G., 2011. The structural basis of inter-individual differences in human behaviour and cognition. Nat. Rev. Neurosci. 12, 231–242.
Karni, A., Meyer, G., Jezzard, P., Adams, M.M., Turner, R., Ungerleider, L.G., 1995. Functional MRI evidence for adult motor cortex plasticity during motor skill learning. Nature 377, 155–158.
Kelly, C., Castellanos, F.X., 2014. Strengthening connections: functional connectivity and brain plasticity. Neuropsychol. Rev. 24, 63–76.
Kerr, A.L., Steuer, E.L., Pochtarev, V., Swain, R.A., 2010. Angiogenesis but not neurogenesis is critical for normal learning and memory acquisition. Neuroscience 171, 214–226.
Kettenmann, H., Kirchhoff, F., Verkhratsky, A., 2013. Microglia: new roles for the synaptic stripper. Neuron 77, 10–18.
Keuken, M.C., Bazin, P.L., Crown, L., Hootsmans, J., Laufer, A., Müller-Axt, C., Sier, R., van der Putten, E.J., Schäfer, A., Turner, R., Forstmann, B.U., 2014. Quantifying inter-individual anatomical variability in the subcortex using 7 T structural MRI. Neuroimage 94, 40–46.
King, B.R., Fogel, S.M., Albouy, G., Doyon, J., 2013. Neural correlates of the age-related changes in motor sequence learning and motor adaptation in older adults. Front. Hum. Neurosci. 7, 142.
Kleim, J.A., Hogg, T.M., VandenBerg, P.M., Cooper, N.R., Bruneau, R., Remple, M., 2004. Cortical synaptogenesis and motor map reorganization occur during late, but not early, phase of motor skill learning. J. Neurosci. 24, 628–633.
Klein, A., Andersson, J., Ardekani, B.A., Ashburner, J., Avants, B., Chiang, M.-C., Christensen, G.E., Collins, D.L., Gee, J., Hellier, P., Song, J.H., Jenkinson, M., Lepage, C., Rueckert, D., Thompson, P., Vercauteren, T., Woods, R.P., Mann, J.J., Parsey, R.V., 2009. Evaluation of 14 nonlinear deformation algorithms applied to human brain MRI registration. Neuroimage 46, 786–802.
Kleinnijenhuis, M., Barth, M., Alexander, D.C., van Cappellen van Walsum, A.M., Norris, D.G., 2012. Structure Tensor Informed Fiber Tractography (STIFT) by combining gradient echo MRI and diffusion weighted imaging. Neuroimage 59, 3941–3954.
Koenig, S.H., Brown, R.D., Adams, D., Emerson, D., Harrison, C.G., 1984. Magnetic field dependence of 1/T1 of protons in tissue. Investig. Radiol. 19, 76–81.
Krieger, S.N., Gauthier, C.J., Ivanov, D., Huber, L., Roggenhofer, E., Sehm, B., Turner, R., Egan, G.F., 2014. Regional reproducibility of calibrated BOLD functional MRI: implications for the study of cognition and plasticity. Neuroimage 101C, 8–20.
Kundu, P., Inati, S.J., Evans, J.W., Luh, W.-M., Bandettini, P.a., 2012. Differentiating BOLD and non-BOLD signals in fMRI time series using multi-echo EPI. Neuroimage 60, 1759–1770.
Kundu, P., Brenowitz, N.D., Voon, V., Worbe, Y., Vértes, P.E., Inati, S.J., Saad, Z.S., Bandettini, P.A., Bullmore, E.T., 2013. Integrated strategy for improving functional connectivity mapping using multiecho fMRI. Proc. Natl. Acad. Sci. U. S. A. 1–6.
Kuo, M.-F., Paulus, W., Nitsche, M.A., 2013. Therapeutic effects of non-invasive brain stimulation with direct currents (tDCS) in neuropsychiatric diseases. Neuroimage 85, 948–960.
Langkammer, C., Krebs, N., Goessler, W., Scheurer, E., Yen, K., Fazekas, F., Ropele, S., 2011. Susceptibility induced gray-white matter MRI contrast in the human brain. Neuroimage 59, 1413–1419.
Lebel, C., Rasmussen, C., Wyper, K., Walker, L., Andrew, G., Yager, J., Beaulieu, C., 2008. Brain diffusion abnormalities in children with fetal alcohol spectrum disorder. Alcohol. Clin. Exp. Res. 32, 1732–1740.
Lee, J., Shmueli, K., Fukunaga, M., van Gelderen, P., Merkle, H., Silva, A.C., Duyn, J.H., 2010. Sensitivity of MRI resonance frequency to the orientation of brain tissue microstructure. Proc. Natl. Acad. Sci. U. S. A. 107, 5130–5135.
Lee, H.L., Zahneisen, B., Hugger, T., LeVan, P., Hennig, J., 2013. Tracking dynamic resting-state networks at higher frequencies using MR-encephalography. Neuroimage 65, 216–222.
Lenglet, C., Abosch, A., Yacoub, E., de Martino, F., Sapiro, G., Harel, N., 2012. Comprehensive in vivo mapping of the human basal ganglia and thalamic connectome in individuals using 7 T MRI. PLoS One 7.
Leontiev, O., Buxton, R.B., 2007. Reproducibility of BOLD, perfusion, and CMRO2 measurements with calibrated-BOLD fMRI. Neuroimage 35, 175–184.
Lerch, J.P., Yiu, A.P., Martinez-Canabal, A., Pekar, T., Bohbot, V.D., Frankland, P.W., Henkelman, R.M., Josselyn, S.a, Sled, J.G., 2011. Maze training in mice induces MRI-detectable brain shape changes specific to the type of learning. Neuroimage 54, 2086–2095.
Lerch, J.P., Gazdzinski, L., Germann, J., Sled, J.G., Henkelman, R.M., Nieman, B.J., 2012. Wanted dead or alive? The tradeoff between in-vivo versus ex-vivo MR brain imaging in the mouse. Front. Neuroinform. 6, 1–9.
Levesque, I.R., Pike, G.B., 2009. Characterizing healthy and diseased white matter using quantitative magnetization transfer and multicomponent T2 relaxometry: a unified view via a four-pool model. Magn. Reson. Med. 62, 1487–1496.
Lewis, C.M., Baldassarre, A., Committeri, G., Romani, G.L., Corbetta, M., 2009. Learning sculpts the spontaneous activity of the resting human brain. Proc. Natl. Acad. Sci. 106, 17558–17563.
Li, T.Q., van Gelderen, P., Merkle, H., Talagala, L., Koretsky, A.P., Duyn, J., 2006. Extensive heterogeneity in white matter intensity in high-resolution T2 *-weighted MRI of the human brain at 7.0 T. Neuroimage 32, 1032–1040.
Li, J., Chang, S., Liu, T., Wang, Q., Cui, D., Chen, X., Jin, M., Wang, B., Pei, M., Wisnieff, C., Spincemaille, P., Zhang, M., Wang, Y., 2012. Reducing the object orientation dependence of susceptibility effects in gradient echo MRI through quantitative susceptibility mapping. Magn. Reson. Med. 68, 1563–1569.
Liao, X.H., Xia, M.R., Xu, T., Dai, Z.J., Cao, X.Y., Niu, H.J., Zuo, X.N., Zang, Y.F., He, Y., 2013. Functional brain hubs and their test-retest reliability: a multiband resting-state functional MRI study. Neuroimage 83, 969–982.
Licht, T., Goshen, I., Avital, A., Kreisel, T., Zubedat, S., Eavri, R., Segal, M., Yirmiya, R., Keshet, E., 2011. Reversible modulations of neuronal plasticity by VEGF. Proc. Natl. Acad. Sci. U. S. A. 108, 5081–5086.
List, J., Kübke, J.C., Lindenberg, R., Külzow, N., Kerti, L., Witte, V., Flöel, A., 2013. Relationship between excitability, plasticity and thickness of the motor cortex in older adults. Neuroimage 83, 809–816.
Liu, T., Khalidov, I., de Rochefort, L., Spincemaille, P., Liu, J., Tsiouris, A.J., Wang, Y., 2011. A novel background field removal method for MRI using projection onto dipole fields (PDF). NMR Biomed. 24, 1129–1136.
Liu, J., Dietz, K., DeLoyht, J.M., Pedre, X., Kelkar, D., Kaur, J., Vialou, V., Lobo, M.K., Dietz, D.M., Nestler, E.J., Dupree, J., Casaccia, P., 2012. Impaired adult myelination in the prefrontal cortex of socially isolated mice. Nat. Neurosci. 15, 1621–1623.
Lövdén, M., Bäckman, L., Lindenberger, U., Schaefer, S., Schmiedek, F., 2010a. A theoretical framework for the study of adult cognitive plasticity. Psychol. Bull. 136, 659–676.
Lövdén, M., Bodammer, N.C., Kühn, S., Kaufmann, J., Schütze, H., Tempelmann, C., Heinze, H.-J., Düzel, E., Schmiedek, F., Lindenberger, U., 2010b. Experience-dependent plasticity of white-matter microstructure extends into old age. Neuropsychologia 48, 3878–3883.
Lövdén, M., Wenger, E., Mårtensson, J., Lindenberger, U., Bäckman, L., 2013. Structural brain plasticity in adult learning and development. Neurosci. Biobehav. Rev. 37, 2296–2310.
Lu, H., Golay, X., Pekar, J.J., Van Zijl, P.C.M., 2003. Functional magnetic resonance imaging based on changes in vascular space occupancy. Magn. Reson. Med. 50, 263–274.
Lüsebrink, F., Wollrab, A., Speck, O., 2013. Cortical thickness determination of the human brain using high resolution 3 T and 7 T MRI data. Neuroimage 70, 122–131.
Lutti, A., Hutton, C., Finsterbusch, J., Helms, G., Weiskopf, N., 2010. Optimization and validation of methods for mapping of the radiofrequency transmit field at 3 T. Magn. Reson. Med. 64, 229–238.
Lutti, A., Dick, F., Sereno, M.I., Weiskopf, N., 2013. Using high-resolution quantitative mapping of R1 as an index of cortical myelination. Neuroimage 93 (Pt 2), 176–188.
Ma, L., Narayana, S., Robin, D.A., Fox, P.T., Xiong, J., 2011. Changes occur in resting state network of motor system during 4 weeks of motor skill learning. Neuroimage 58, 226–233.
MacKay, A., Whittall, K., Adler, J., Li, D., Paty, D., Graeb, D., 1994. In vivo visualization of myelin water in brain by magnetic resonance. Magn. Reson. Med. 31, 673–677.
Mackey, A.P., Singley, A.T.M., Bunge, S.A., 2013. Intensive reasoning training alters patterns of brain connectivity at rest. J. Neurosci. 33, 4796–4803.
Maguire, E.A., Gadian, D.G., Johnsrude, I.S., Good, C.D., Ashburner, J., Frackowiak, R.S., Frith, C.D., 2000. Navigation-related structural change in the hippocampi of taxi drivers. Proc. Natl. Acad. Sci. U. S. A. 97, 4398–4403.
Marques, J.P., Kober, T., Krueger, G., van der Zwaag, W., Van de Moortele, P.F., Gruetter, R., 2010. MP2RAGE, a self bias-field corrected sequence for improved segmentation and T1-mapping at high field. Neuroimage 49, 1271–1281.
May, A., 2011. Experience-dependent structural plasticity in the adult human brain. Trends Cogn. Sci. 15, 475–482.
McNab, J.A., Edlow, B.L., Witzel, T., Huang, S.Y., Bhat, H., Heberlein, K., Feiweier, T., Liu, K., Keil, B., Cohen-Adad, J., Tisdall, M.D., Folkerth, R.D., Kinney, H.C., Wald, L.L., 2013. The

Human Connectome Project and beyond: initial applications of 300mT/m gradients. Neuroimage 80, 234–245.
Metere, R., Möller, H.E., Krüger, G., Kober, T., Schäfer, A., 2015. Simultaneous Quantitative Mapping of T1 , T2*, and Magnetic Susceptibility with Multi-Echo MP2RAGE at 7 T. 23rd Annual Meeting of the International Society for Magnetic Resonance in Medicine (ISMRM). Toronto, Canada.
Mezer, A., Yeatman, J.D., Stikov, N., Kay, K.N., Cho, N.-J., Dougherty, R.F., Perry, M.L., Parvizi, J., Hua, L.H., Butts-Pauly, K., Wandell, B.A., 2013. Quantifying the local tissue volume and composition in individual brains with magnetic resonance imaging. Nat. Med. 19, 1667–1672.
Miller, M.I., 2004. Computational anatomy: shape, growth, and atrophy comparison via diffeomorphisms. Neuroimage S19–S33.
Moeller, S., Yacoub, E., Olman, C.A., Auerbach, E., Strupp, J., Harel, N., Uğurbil, K., 2010. Multiband multislice GE-EPI at 7 Tesla, with 16-fold acceleration using partial parallel imaging with application to high spatial and temporal whole-brain FMRI. Magn. Reson. Med. 63, 1144–1153.
Mohammadi, S., Tabelow, K., Ruthotto, L., Feiweier, T., Polzehl, J., Weiskopf, N., 2014. High-resolution diffusion kurtosis imaging at 3 T enabled by advanced post-processing. Front. Neurosci. 8, 427.
Mori, S., Kaufmann, W.E., Davatzikos, C., Stieltjes, B., Amodei, L., Fredericksen, K., Pearlson, G.D., Melhem, E.R., Solaiyappan, M., Raymond, G.V., Moser, H.W., Van Zijl, P.C.M., 2002. Imaging cortical association tracts in the human brain using diffusion-tensor-based axonal tracking. Magn. Reson. Med. 47, 215–223.
Mougin, O.E., Coxon, R.C., Pitiot, A., Gowland, P.A., 2010. Magnetization transfer phenomenon in the human brain at 7 T. Neuroimage 49, 272–281.
Mozolic, J.L., Hayasaka, S., Laurienti, P.J., 2010. A cognitive training intervention increases resting cerebral blood flow in healthy older adults. Front. Hum. Neurosci. 4, 16.
Mugler III, J.P., Brookeman, J.R., 1990. Three-dimensional magnetization-prepared rapid gradient-echo imaging (3D MP-RAGE). Magn. Reson. Med. 15, 152–157.
Murphy, K., Harris, A.D., Diukova, A., Evans, C.J., Lythgoe, D.J., Zelaya, F., Wise, R.G., 2011. Pulsed arterial spin labeling perfusion imaging at 3 T: estimating the number of subjects required in common designs of clinical trials. Magn. Reson. Imaging 29, 1382–1389.
Murphy, T., Dias, G.P., Thuret, S., 2014. Effects of diet on brain plasticity in animal and human studies: mind the gap. Neural Plast. 2014, 1–32.
Ng, A., Johnston, L., Chen, Z., Cho, Z.H., Zhang, J., Egan, G., 2011. Spatially dependent filtering for removing phase distortions at the cortical surface. Magn. Reson. Med. 66, 784–793.
O'Donnell, L.J., Westin, C.F., Golby, A.J., 2009. Tract-based morphometry for white matter group analysis. Neuroimage 45, 832–844.
Pajevic, S., Basser, P.J., Fields, R.D., 2014. Role of myelin plasticity in oscillations and synchrony of neuronal activity. Neuroscience 276, 135–147.
Pampel, A., Müller, D.K., Anwander, A., Marschner, H., Möller, H.E., 2015. Orientation dependence of magnetization transfer parameters in human white matter. Neuroimage 114, 136–146.
Park, M.T.M., Pipitone, J., Baer, L.H., Winterburn, J.L., Shah, Y., Chavez, S., Schira, M.M., Lobaugh, N.J., Lerch, J.P., Voineskos, A.N., Chakravarty, M.M., 2014. Derivation of high-resolution MRI atlases of the human cerebellum at 3 T and segmentation using multiple automatically generated templates. Neuroimage 95, 217–231.
Parsons, E.C., Does, M.D., Gore, J.C., 2006. Temporal diffusion spectroscopy: theory and implementation in restricted systems using oscillating gradients. Magn. Reson. Med. 55, 75–84.
Pasternak, O., Sochen, N., Gur, Y., Intrator, N., Assaf, Y., 2009. Free water elimination and mapping from diffusion MRI. Magn. Reson. Med. 62, 717–730.
Pasternak, O., Westin, C.-F., Bouix, S., Seidman, L.J., Goldstein, J.M., Woo, T.-U.W., Petryshen, T.L., Mesholam-Gately, R.I., McCarley, R.W., Kikinis, R., Shenton, M.E., Kubicki, M., 2012. Excessive extracellular volume reveals a neurodegenerative pattern in schizophrenia onset. J. Neurosci. 32, 17365–17372.
Pearson-Fuhrhop, K.M., Cramer, S.C., 2010. Genetic influences on neural plasticity. PM&R 2, S227–S240.
Pereira, A.C., Huddleston, D.E., Brickman, A.M., Sosunov, A.A., Hen, R., McKhann, G.M., Sloan, R., Gage, F.H., Brown, T.R., Small, S.A., 2007. An in vivo correlate of exercise-induced neurogenesis in the adult dentate gyrus. Proc. Natl. Acad. Sci. U. S. A. 104, 5638–5643.
Peters, A., 2009. The effects of normal aging on myelinated nerve fibers in monkey central nervous system. Front. Neuroanat. 3, 11.
Peters, A.M., Brookes, M.J., Hoogenraad, F.G., Gowland, P.A., Francis, S.T., Morris, P.G., Bowtell, R., 2007. T2* measurements in human brain at 1.5, 3 and 7 T. Magn. Reson. Imaging 25, 748–753.
Pohmann, R., Scheffler, K., 2013. A theoretical and experimental comparison of different techniques for B1 mapping at very high fields. NMR Biomed. 26, 265–275.
Polanía, R., Paulus, W., Nitsche, M.A., 2012. Reorganizing the intrinsic functional architecture of the human primary motor cortex during rest with non-invasive cortical stimulation. PLoS One 7, e30971.
Portnoy, S., Stanisz, G.J., 2007. Modeling pulsed magnetization transfer. Magn. Reson. Med. 58, 144–155.
Power, J.D., Cohen, A.L., Nelson, S.M., Wig, G.S., Barnes, K.A., Church, J.A., Vogel, A.C., Laumann, T.O., Miezin, F.M., Schlaggar, B.L., Petersen, S.E., 2011. Functional network organization of the human brain. Neuron 72, 665–678.
Power, J.D., Mitra, A., Laumann, T.O., Snyder, A.Z., Schlaggar, B.L., Petersen, S.E., 2014. Methods to detect, characterize, and remove motion artifact in resting state fMRI. Neuroimage 84, 320–341.
Preibisch, C., Deichmann, R., 2009. Influence of RF spoiling on the stability and accuracy of T1 mapping based on spoiled FLASH with varying flip angles. Magn. Reson. Med. 61, 125–135.
Rack-Gomer, A.L., Liau, J., Liu, T.T., 2009. Caffeine reduces resting-state BOLD functional connectivity in the motor cortex. Neuroimage 46, 56–63.
Raffelt, D., Tournier, J.D., Rose, S., Ridgway, G.R., Henderson, R., Crozier, S., Salvado, O., Connelly, A., 2012. Apparent fibre density: a novel measure for the analysis of diffusion-weighted magnetic resonance images. Neuroimage 59, 3976–3994.
Rajab, A.S., Crane, D.E., Middleton, L.E., Robertson, A.D., Hampson, M., Macintosh, B.J., 2014. A single session of exercise increases connectivity in sensorimotor-related brain networks : a resting-state fMRI study in young healthy adults. Front. Hum. Neurosci. 8, 1–9.
Riffert, T.W., Schreiber, J., Anwander, A., Knösche, T.R., 2014. Beyond fractional anisotropy: extraction of bundle-specific structural metrics from crossing fiber models. Neuroimage 100, 176–191.
Rioult-Pedotti, M.S., Friedman, D., Donoghue, J.P., 2000. Learning-induced LTP in neocortex. Science 290, 533–536.
Robinson, E.C., Jbabdi, S., Glasser, M.F., Andersson, J., Burgess, G.C., Harms, M.P., Smith, S.M., Van Essen, D.C., Jenkinson, M., 2014. MSM: a new flexible framework for multimodal surface matching. Neuroimage 100, 414–426.
Rooney, W.D., Johnson, G., Li, X., Cohen, E.R., Kim, S.G., Ugurbil, K., Springer, C.S., 2007. Magnetic field and tissue dependencies of human brain longitudinal 1H2O relaxation in vivo. Magn. Reson. Med. 57, 308–318.
Rosenzweig, M.R., Krech, D., Bennett, E.L., Diamond, M.C., 1962. Effects of environmental complexity and training on brain chemistry and antomy: a replication and extension. J. Comp. Physiol. Psychol. 55, 429–437.
Rudko, D.A., Klassen, L.M., de Chickera, S.N., Gati, J.S., Dekaban, G.A., Menon, R.S., 2014. Origins of R2* orientation dependence in gray and white matter. Proc. Natl. Acad. Sci. U. S. A. 111, E159–E167.
Ryali, S., Chen, T., Supekar, K., Menon, V., 2012. Estimation of functional connectivity in fMRI data using stability selection-based sparse partial correlation with elastic net penalty. Neuroimage 59, 3852–3861.
Sagi, Y., Tavor, I., Hofstetter, S., Tzur-Moryosef, S., Blumenfeld-Katzir, T., Assaf, Y., 2012. Learning in the fast lane: new insights into neuroplasticity. Neuron 73, 1195–1203.
Sampaio-Baptista, C., Khrapitchev, A.A., Foxley, S., Schlagheck, T., Scholz, J., Jbabdi, S., Deluca, G.C., Miller, K.L., Taylor, A., Thomas, N., Kleim, J., Sibson, N.R., Bannerman, D., Johansen-Berg, H., 2013. Motor skill learning induces changes in white matter microstructure and myelination. J. Neurosci. 33, 19499–19503.
Sampaio-Baptista, C., Scholz, J., Jenkinson, M., Thomas, A.G., Filippini, N., Smit, G., Douaud, G., Johansen-Berg, H., 2014. Gray matter volume is associated with rate of subsequent skill learning after a long term training intervention. Neuroimage 96, 158–166.
Satterthwaite, T.D., Elliott, M.A., Gerraty, R.T., Ruparel, K., Loughead, J., Calkins, M.E., Eickhoff, S.B., Hakonarson, H., Gur, R.C., Gur, R.E., 2013. An improved framework for confound regression and filtering for control of motion artifact in the preprocessing of resting-state functional connectivity data. Neuroimage 64, 240–256.
Schäfer, A., Wharton, S., Gowland, P., Bowtell, R., 2009. Using magnetic field simulation to study susceptibility-related phase contrast in gradient echo MRI. Neuroimage 48, 126–137.
Schlaug, G., Jäncke, L., Huang, Y., Staiger, J.F., Steinmetz, H., 1995. Increased corpus callosum size in musicians. Neuropsychologia 33, 1047–1055.
Schmidt-Wilcke, T., Rosengarth, K., Luerding, R., Bogdahn, U., Greenlee, M.W., 2010. Distinct patterns of functional and structural neuroplasticity associated with learning Morse code. Neuroimage 51, 1234–1241.
Schmierer, K., Wheeler-Kingshott, C.A., Tozer, D.J., Boulby, P.A., Parkes, H.G., Yousry, T.A., Scaravilli, F., Barker, G.J., Tofts, P.S., Miller, D.H., 2008. Quantitative magnetic resonance of postmortem multiple sclerosis brain before and after fixation. Magn. Reson. Med. 59, 268–277.
Schmierer, K., Thavarajah, J.R., An, S.F., Brandner, S., Miller, D.H., Tozer, D.J., 2010. Effects of formalin fixation on magnetic resonance indices in multiple sclerosis cortical gray matter. J. Magn. Reson. Imaging 32, 1054–1060.
Scholz, J., Klein, M.C., Behrens, T.E.J., Johansen-Berg, H., 2009. Training induces changes in white-matter architecture. Nat. Neurosci. 12, 1370–1371.
Scholz, J., Niibori, Y., Frankland, P., Lerch, J., 2014. Rotarod training in mice is associated with changes in brain structure observable with multimodal MRI. Neuroimage 107, 182–189.
Scholz, J., Allemang-Grand, R., Dazai, J., Lerch, J.P., 2015. Environmental enrichment is associated with rapid volumetric brain changes in adult mice. Neuroimage 109, 190–198.
Schreiber, J., Riffert, T., Anwander, A., Knösche, T.R., 2014. Plausibility tracking: a method to evaluate anatomical connectivity and microstructural properties along fiber pathways. Neuroimage 90, 163–178.
Schweser, F., Deistung, A., Lehr, B.W., Reichenbach, J.R., 2011. Quantitative imaging of intrinsic magnetic tissue properties using MRI signal phase: an approach to in vivo brain iron metabolism? Neuroimage 54, 2789–2807.
Schweser, F., Deistung, A., Sommer, K., Reichenbach, J.R., 2013. Toward online reconstruction of quantitative susceptibility maps: superfast dipole inversion. Magn. Reson. Med. 69, 1582–1594.
Sehm, B., Schäfer, A., Kipping, J.A., Margulies, D.S., Conde, V., Taubert, M., Villringer, A., Ragert, P., 2012. Dynamic modulation of intrinsic functional connectivity by transcranial direct current stimulation. J. Neurophysiol. 108, 3253–3263.
Sereno, M.I., Lutti, A., Weiskopf, N., Dick, F., 2013. Mapping the human cortical surface by combining quantitative T1 with retinotopy. Cereb. Cortex 23, 2261–2268.
Setsompop, K., Cohen-Adad, J., Gagoski, B.A., Raij, T., Yendiki, A., Keil, B., Wedeen, V.J., Wald, L.L., 2012. Improving diffusion MRI using simultaneous multi-slice echo planar imaging. Neuroimage 63, 569–580.
Shmuel, A., Leopold, D.A., 2008. Neuronal correlates of spontaneous fluctuations in fMRI signals in monkey visual cortex: implications for functional connectivity at rest. Hum. Brain Mapp. 29, 751–761.

Sirevaag, A.M., Black, J.E., Shafron, D., Greenough, W.T., 1988. Direct evidence that complex experience increases capillary branching and surface area in visual cortex of young rats. Brain Res. 471, 299–304.

Sled, J.G., Pike, G.B., 2001. Quantitative imaging of magnetization transfer exchange and relaxation properties in vivo using MRI. Magn. Reson. Med. 46, 923–931.

Smith, S.M., Jenkinson, M., Johansen-Berg, H., Rueckert, D., Nichols, T.E., Mackay, C.E., Watkins, K.E., Ciccarelli, O., Cader, M.Z., Matthews, P.M., Behrens, T.E.J., 2006. Tract-based spatial statistics: voxelwise analysis of multi-subject diffusion data. Neuroimage 31, 1487–1505.

Smith, S.M., Miller, K.L., Salimi-Khorshidi, G., Webster, M., Beckmann, C.F., Nichols, T.E., Ramsey, J.D., Woolrich, M.W., 2011. Network modelling methods for FMRI. Neuroimage 54, 875–891.

Soares, J.M., Sampaio, A., Ferreira, L.M., Santos, N.C., Marques, P., Marques, F., Palha, J.A., Cerqueira, J.J., Sousa, N., 2013. Stress impact on resting state brain networks. PLoS One 8, e66500.

Song, S.-K., Sun, S.-W., Ramsbottom, M.J., Chang, C., Russell, J., Cross, A.H., 2002. Dysmyelination revealed through MRI as increased radial (but unchanged axial) diffusion of water. Neuroimage 17, 1429–1436.

Sotiropoulos, S.N., Behrens, T.E.J., Jbabdi, S., 2012. Ball and rackets: inferring fiber fanning from diffusion-weighted MRI. Neuroimage 60, 1412–1425.

Steele, C.J., Penhune, V.B., 2010. Specific increases within global decreases: a functional magnetic resonance imaging investigation of five days of motor sequence learning. J. Neurosci. 30, 8332–8341.

Steele, C.J., Bailey, J.A., Zatorre, R.J., Penhune, V.B., 2013. Early musical training and white-matter plasticity in the corpus callosum: evidence for a sensitive period. J. Neurosci. 33, 1282–1290.

Stefan, K., Kunesch, E., Cohen, L.G., Benecke, R., Classen, J., 2000. Induction of plasticity in the human motor cortex by paired associative stimulation. Brain 123 (Pt 3), 572–584.

Stevens, B., Porta, S., Haak, L.L., Gallo, V., Fields, R.D., 2002. Adenosine: a neuron-glial transmitter promoting myelination in the CNS in response to action potentials. Neuron 36, 855–868.

Stikov, N., Boudreau, M., Levesque, I.R., Tardif, C.L., Barral, J.K., Pike, G.B., 2014. On the accuracy of T1 mapping: searching for common ground. Magn. Reson. Med. 00, 1–9.

Stikov, N., Campbell, J.S.W., Stroh, T., Lavelée, M., Frey, S., Novek, J., Nuara, S., Ho, M.-K., Bedell, B.J., Dougherty, R.F., Leppert, I.R., Boudreau, M., Narayanan, S., Duval, T., Cohen-Adad, J., Picard, P., Gasecka, A., Côté, D., Bruce Pike, G., 2015. In vivo histology of the myelin g-ratio with magnetic resonance imaging. Neuroimage 118, 397–405.

Stüber, C., Morawski, M., Schäfer, A., Labadie, C., Wähnert, M., Leuze, C., Streicher, M., Barapatre, N., Reimann, K., Geyer, S., Spemann, D., Turner, R., 2014. Myelin and iron concentration in the human brain: a quantitative study of MRI contrast. Neuroimage 93, 95–106.

Supekar, K., Swigart, A.G., Tenison, C., Jolles, D.D., Rosenberg-Lee, M., Fuchs, L., Menon, V., 2013. Neural predictors of individual differences in response to math tutoring in primary-grade school children. Proc. Natl. Acad. Sci. U. S. A. 110, 8230–8235.

Tardif, C.L., Schäfer, A., Waehnert, M., Dinse, J., Turner, R., Bazin, P.-L., 2015. Multi-contrast multi-scale surface registration for improved alignment of cortical areas. Neuroimage 111, 107–122.

Taubert, M., Draganski, B., Anwander, A., Müller, K., Horstmann, A., Villringer, A., Ragert, P., 2010. Dynamic properties of human brain structure: learning-related changes in cortical areas and associated fiber connections. J. Neurosci. 30, 11670–11677.

Taubert, M., Lohmann, G., Margulies, D.S., Villringer, A., Ragert, P., 2011. Long-term effects of motor training on resting-state networks and underlying brain structure. Neuroimage 57, 1492–1498.

Taubert, M., Villringer, A., Ragert, P., 2012. Learning-related gray and white matter changes in humans: an update. Neuroscientist 18, 320–325.

Theodosis, D.T., Poulain, D.a, Oliet, S.H.R., 2008. Activity-dependent structural and functional plasticity of astrocyte-neuron interactions. Physiol. Rev. 88, 983–1008.

Thomas, C., Baker, C.I., 2013. Teaching an adult brain new tricks: a critical review of evidence for training-dependent structural plasticity in humans. Neuroimage 73, 225–236.

Thomas, A.G., Dennis, A., Bandettini, P.a, Johansen-Berg, H., 2012. The effects of aerobic activity on brain structure. Front. Psychol. 3, 86.

Thompson, W.K., Holland, D., 2011. Bias in tensor based morphometry Stat-ROI measures may result in unrealistic power estimates. Neuroimage 57, 1–4.

Todorich, B., Pasquini, J.M., Garcia, C.I., Paez, P.M., Connor, J.R., 2009. Oligodendrocytes and myelination: the role of iron. Glia 57, 467–478.

Todorich, B., Zhang, X., Connor, J.R., 2011. H-ferritin is the major source of iron for oligodendrocytes. Glia 59, 927–935.

Tofts, P., 2003. Quantitative MRI of the Brain: Measuring Changes Caused by Disease. John Wiley & Sons Ltd., Chichester, West Sussex, England.

Topfer, R., Schweser, F., Deistung, A., Reichenbach, J.R., Wilman, A.H., 2015. SHARP edges: recovering cortical phase contrast through harmonic extension. Magn. Reson. Med. 73, 851–856.

Tosun, D., Siddarth, P., Toga, A.W., Hermann, B., Caplan, R., 2011. Effects of childhood absence epilepsy on associations between regional cortical morphometry and aging and cognitive abilities. Hum. Brain Mapp. 32, 580–591.

Tournier, J.-D., Calamante, F., Connelly, A., 2007. Robust determination of the fibre orientation distribution in diffusion MRI: non-negativity constrained super-resolved spherical deconvolution. Neuroimage 35, 1459–1472.

Tournier, J.-D., Mori, S., Leemans, A., 2011. Diffusion tensor imaging and beyond. Magn. Reson. Med. 65, 1532–1556.

Tronel, S., Fabre, A., Charrier, V., Oliet, S.H.R., Gage, F.H., Abrous, D.N., 2010. Spatial learning sculpts the dendritic arbor of adult-born hippocampal neurons. Proc. Natl. Acad. Sci. U. S. A. 107, 7963–7968.

Turner, R., 2014. Comparing Like with Like: The Power of Knowing Where You Are. Brain Connect. 4, 547–557.

Valkanova, V., Eguia Rodriguez, R., Ebmeier, K.P., 2014. Mind over matter—what do we know about neuroplasticity in adults? Int. Psychogeriatr. 26, 891–909.

Van de Moortele, P.F., Auerbach, E.J., Olman, C., Yacoub, E., Uğurbil, K., Moeller, S., 2009. T1 weighted brain images at 7 Tesla unbiased for proton density, T2 * contrast and RF coil receive B1 sensitivity with simultaneous vessel visualization. Neuroimage 46, 432–446.

Van Dijk, K.R.A., Sabuncu, M.R., Buckner, R.L., 2012. The influence of head motion on intrinsic functional connectivity MRI. Neuroimage 59, 431–438.

Varoquaux, G., Craddock, R., 2013. Learning and comparing functional connectomes across subjects. Neuroimage 80, 405–415.

Varoquaux, G., Gramfort, A., Poline, J.B., Thirion, B., 2010. Brain covariance selection: better individual functional connectivity models using population prior. Adv. Neural Inf. Process. Syst. 2334–2342.

Voelcker-Rehage, C., Niemann, C., 2013. Structural and functional brain changes related to different types of physical activity across the life span. Neurosci. Biobehav. Rev. 37, 2268–2295.

Voineskos, A.N., Winterburn, J.L., Felsky, D., Pipitone, J., Rajji, T.K., Mulsant, B.H., Chakravarty, M.M., 2015. Hippocampal (subfield) volume and shape in relation to cognitive performance across the adult lifespan. Hum. Brain Mapp. 36, 3020–3037.

Volz, S., Nöth, U., Jurcoane, A., Ziemann, U., Hattingen, E., Deichmann, R., 2012. Quantitative proton density mapping: correcting the receiver sensitivity bias via pseudo proton densities. Neuroimage 63, 540–552.

Voss, P., Zatorre, R.J., 2012. Occipital cortical thickness predicts performance on pitch and musical tasks in blind individuals. Cereb. Cortex 22, 2455–2465.

Voss, M.W., Prakash, R.S., Erickson, K.I., Basak, C., Chaddock, L., Kim, J.S., Alves, H., Heo, S., Szabo, A.N., White, S.M., Wójcicki, T.R., Mailey, E.L., Gothe, N., Olson, E.A., McAuley, E., Kramer, A.F., 2010. Plasticity of brain networks in a randomized intervention trial of exercise training in older adults. Front. Aging Neurosci. 2.

Voss, M.W., Prakash, R.S., Erickson, K.I., Boot, W.R., Basak, C., Neider, M.B., Simons, D.J., Fabiani, M., Gratton, G., Kramer, A.F., 2012. Effects of training strategies implemented in a complex videogame on functional connectivity of attentional networks. Neuroimage 59, 138–148.

Voss, M.W., Vivar, C., Kramer, A.F., van Praag, H., 2013. Bridging animal and human models of exercise-induced brain plasticity. Trends Cogn. Sci. 17, 525–544.

Voss, P., Pike, B.G., Zatorre, R.J., 2014. Evidence for both compensatory plastic and disuse atrophy-related neuroanatomical changes in the blind. Brain 137, 1224–1240.

Wake, H., Lee, P.R., Fields, R.D., 2011. Control of local protein synthesis and initial events in myelination by action potentials. Science 333, 1647–1651.

Wang, Y., Liu, T., 2015. Quantitative susceptibility mapping (QSM): decoding MRI data for a tissue magnetic biomarker. Magn. Reson. Med. 73, 82–101.

Weiskopf, N., Suckling, J., Williams, G., Correia, M.M., Inkster, B., Tait, R., Ooi, C., Bullmore, E.T., Lutti, A., 2013a. Quantitative multi-parameter mapping of R1, PD(*), MT, and R2(*) at 3 T: a multi-center validation. Front. Neurosci. 7, 95.

Weiskopf, N., Suckling, J., Williams, G., Correia, M.M., Inkster, B., Tait, R., Ooi, C., Bullmore, E.T., Lutti, A., 2013b. Quantitative multi-parameter mapping of R1, PD*, MT, and R2* at 3 T: a multi-center validation. Front. Neurosci. 7.

Weissenbacher, A., Kasess, C., Gerstl, F., Lanzenberger, R., Moser, E., Windischberger, C., 2009. Correlations and anticorrelations in resting-state functional connectivity MRI: a quantitative comparison of preprocessing strategies. Neuroimage 47, 1408–1416.

West, J., Warntjes, J.B.M., Lundberg, P., 2012. Novel whole brain segmentation and volume estimation using quantitative MRI. Eur. Radiol. 22, 998–1007.

Wharton, S., Bowtell, R., 2012. Fiber orientation-dependent white matter contrast in gradient echo MRI. Proc. Natl. Acad. Sci. 109, 18559–18564.

Wharton, S., Bowtell, R., 2015. Effects of white matter microstructure on phase and susceptibility maps. Magn. Reson. Med. 73, 1258–1269.

Wig, G.S., Laumann, T.O., Petersen, S.E., 2013. An approach for parcellating human cortical areas using resting-state correlations. Neuroimage 1–16.

Wise, R.G., Harris, A.D., Stone, A.J., Murphy, K., 2013. Measurement of OEF and absolute CMRO: MRI-based methods using interleaved and combined hypercapnia and hyperoxia. Neuroimage 83C, 135–147.

Wolff, S.D., Balaban, R.S., 1989. Magnetization transfer contrast (MTC) and tissue water proton relaxation in vivo. Magn. Reson. Med. 10, 135–144.

Wu, E.X., Cheung, M.M., 2010. MR diffusion kurtosis imaging for neural tissue characterization. NMR Biomed. 23, 836–848.

Xu, T., Yu, X., Perlik, A.J., Tobin, W.F., Zweig, J.A., Tennant, K., Jones, T., Zuo, Y., 2009. Rapid formation and selective stabilization of synapses for enduring motor memories. Nature 462, 915–919.

Xu, J., Li, H., Harkins, K.D., Jiang, X., Xie, J., Kang, H., Does, M.D., Gore, J.C., 2014. Mapping mean axon diameter and axonal volume fraction by MRI using temporal diffusion spectroscopy. Neuroimage 103, 10–19.

Yarnykh, V.L., 2010. Optimal radiofrequency and gradient spoiling for improved accuracy of T1 and B1 measurements using fast steady-state techniques. Magn. Reson. Med. 63, 1610–1626.

Yeo, B.T.T., Krienen, F.M., Sepulcre, J., Sabuncu, M.R., Lashkari, D., Hollinshead, M., Roffman, J.L., Smoller, J.W., Zöllei, L., Polimeni, J.R., Fischl, B., Liu, H., Buckner, R.L., 2011. The organization of the human cerebral cortex estimated by intrinsic functional connectivity. J. Neurophysiol. 106, 1125–1165.

Younes, L., 2010. Shapes and Diffeomorphisms. Springer, Berlin Heidelberg.

Young, K.M., Psachoulia, K., Tripathi, R.B., Dunn, S.J., Cossell, L., Attwell, D., Tohyama, K., Richardson, W.D., 2013. Oligodendrocyte dynamics in the healthy adult CNS: evidence for myelin remodeling. Neuron 77, 873–885.

Young, B.M., Nigogosyan, Z., Remsik, A., Walton, Lã©.M., Song, J., Nair, V.A., Grogan, S.W., Tyler, M.E., Edwards, D.F., Caldera, K., Sattin, J.A., Williams, J.C., Prabhakaran, V., 2014. Changes in functional connectivity correlate with behavioral gains in stroke patients after therapy using a brain-computer interface device. Front. Neuroeng. 7, 1–12.

Yuen, T.J., Silbereis, J.C., Griveau, A., Chang, S.M., Daneman, R., Fancy, S.P.J., Zahed, H., Maltepe, E., Rowitch, D.H., 2014. Oligodendrocyte-encoded HIF function couples postnatal myelination and white matter angiogenesis. Cell 158, 383–396.

Yushkevich, P.A., Avants, B.B., Das, S.R., Pluta, J., Altinay, M., Craige, C., 2010. Bias in estimation of hippocampal atrophy using deformation-based morphometry arises from asymmetric global normalization: an illustration in ADNI 3 T MRI data. Neuroimage 50, 434–445.

Zatorre, R.J., Fields, R.D., Johansen-Berg, H., 2012. Plasticity in gray and white: neuroimaging changes in brain structure during learning. Nat. Neurosci. 15, 528–536.

Zechariah, A., ElAli, A., Doeppner, T.R., Jin, F., Hasan, M.R., Helfrich, I., Mies, G., Hermann, D.M., 2013. Vascular endothelial growth factor promotes pericyte coverage of brain capillaries, improves cerebral blood flow during subsequent focal cerebral ischemia, and preserves the metabolic penumbra. Stroke 44, 1690–1697.

Zhang, H., Schneider, T., Wheeler-Kingshott, C.A., Alexander, D.C., 2012. NODDI: practical in vivo neurite orientation dispersion and density imaging of the human brain. Neuroimage 61, 1000–1016.